LRP 583/97 November 1997

THE SEPARATRIX RESPONSE OF DIVERTED TCV PLASMAS COMPARED TO THE CREATE-L MODEL

P. Vyas, F. Villone, J.B. Lister, R. Albanese

THE SEPARATRIX RESPONSE OF DIVERTED TCV PLASMAS COMPARED TO THE CREATE-L MODEL

P. Vyas, F. Villone[1], J.B. Lister, R. Albanese[2]

Centre de Recherches en Physique des Plasmas,
Association EURATOM-Confédération Suisse,
Ecole Polytechnique Fédérale de Lausanne,
Lausanne, Switzerland

[1]Associazione EURATOM/ENEA/CREATE,
Dipartimento di Ingegneria Industriale,
Università degli Studi di Cassino,
Cassino (FR), Italy

[2]Associazione EURATOM/ENEA/CREATE,
DIEMA,
Università di Reggio Calabria,
Reggio Calabria, Italy

ABSTRACT

The response of Ohmic, single-null diverted, non-centred plasmas in TCV to poloidal field coil stimulation has been compared to the linear CREATE-L MHD equilibrium response model. The closed loop responses of directly measured quantities, reconstructed parameters, and the reconstructed plasma contour were all examined. Provided that the plasma position and shape perturbation were small enough for the linearity assumption to hold, the model-experiment agreement was good. For some stimulations the open loop vertical position instability growth rate changed significantly, illustrating the limitations of a linear model.

A different model was developed with the assumption that the flux at the plasma boundary is frozen and was also compared with experimental results. It proved not to be as reliable as the CREATE-L model for some simulation parameters showing that the experiments were able to discriminate between different plasma response models. The closed loop response was also found to be sensitive to changes in the modelled plasma shape. It was not possible to invalidate the CREATE-L model despite the extensive range of responses excited by the experiments.

1. INTRODUCTION

Many attempts have been made to model the plasma position and shape response in tokamaks. A variety of phenomenological models have been developed ranging from simple single current filament models for the plasma vertical position to complicated nonlinear time-varying codes. The accuracy of these models has generally been sufficient to develop the relatively simple but reliable PID based controllers for poloidal field coil systems. Recent work on tokamak controller design using modern control theory has increased attention on these models. Modern control techniques are often based on the optimization of a controller given a model of the plant. When implemented the achieved performance of such controllers then depends on the accuracy of the model. Validation of these models is increasing in importance given the proposed use of advanced model-based controllers for ITER.

The closed loop time domain responses of a symmetric, centred, limited TCV plasma to coil voltage stimulation were previously compared to a rigid current displacement model (RCDM) in [1]. Square pulses and random binary sequences (RBS) were applied to the poloidal field coils to excite only the plasma vertical position. The model agreement was found to be good and showed that the coils close to the centre on the inboard side were best coupled to the fast vertical motion of the plasma. The RBS data was analyzed to produce frequency response estimates which were compared with both the RCDM and a simplified CREATE-L model in [2]. The frequency responses of both models agreed with the measured responses. It was confirmed that coil-pair E4-E5 has a much larger closed loop amplitude response at frequencies above 10Hz than the pair F1-F8 and has a smaller phase lag (Fig. 1).

Up-down symmetric excitation in TCV, first introduced in [2], was used to examine the response of up-down symmetric parameters. The plasma shape and position was stimulated with a wide variety of signals using the extensive poloidal field coil set of TCV. The RCDM cannot model these outputs and instead the simplified CREATE-L model and a plasmaless CREATE-L model were compared to the experiment. Since the design of the TCV controller used for the symmetric variables was based on a plasmaless model the latter was thought also to be useful for comparison.

This paper extends this work to address questions unanswered in the previous papers. The primary restriction of limited, up-down symmetric, centred plasmas has been removed by using a single-null diverted (SND), non-centred plasma. Figure 1 shows the TCV vacuum vessel along with the active coil set and magnetic probes. The nominal

plasma contour before any stimulation is also represented. The chosen plasma parameters were κ=1.44, δ=0.38, R_p=0.89m, I_p=200kA and q_a=7.3. The up-down coil pairs used previously no longer have the same separation between zI_p and other parameters, so the work was naturally extended to single coil excitation. The choice of parameters under feedback control was also simplified to I_p, vertical flux imbalance (radial position) and zI_p only. The results of model-experiment comparisons for directly measured quantities are presented in Section 2.

The possibility that surface currents may occur is also introduced. Since the CREATE-L model assumes no surface currents, maintaining a fixed current profile shape, the effect of this assumption can be tested. Single coil excitation introduces a tilting motion to the plasma shape leading to more complicated shape responses than tested before. Some observations not seen previously are also raised in this paper. One issue is the nonlinear coupling of the zI_p dynamics to changes in radial position. The implications for the prediction of loop stability and the importance of controller robustness to changes in open loop instability growth rate are discussed.

A further extension to the previous work is the questioning of some of the physics assumptions in the CREATE-L model. In total six CREATE-L models plus the RCDM are examined in this paper. Alongside the plasmaless model, there is the benchmark model for the SND plasma which will be referred to simply as the CREATE-L model. This model is an extension of the *simplified* CREATE-L model used in [2], in that the poloidal and toroidal magnetic field coupling and the pressure work are now taken into account, as described in [3]. The effects of the additional terms are negligible, since the results provided by the two models are indistinguishable. Two other models are also compared with the experimental data in Section 2. One was generated using the same equations for a plasma of similar shape but limited instead of diverted (Fig. 1), and is referred to here as the *limited* CREATE-L model. A different model based on the assumption of frozen poloidal flux at the plasma boundary (the *frozen flux* CREATE-L model) was also examined. These last two models allow us to test the sensitivity of the plasma model responses to different assumptions on the plasma boundary flux. Indeed, in the CREATE-L model we assume the boundary flux as the flux at the nominal X-point, whereas the limited CREATE-L model keeps the nominal plasma-wall contact point flux as the boundary flux. Since the sensitivity of the model to the radial position is particularly acute, as is discussed in the following, we also produced two additional models for a plasma shifted slightly radially outward. These two models are referred to as the *shifted* CREATE-L and the *shifted frozen flux* CREATE-L models.

The proposed ITER controller defines gaps around the contour of the plasma as the control parameters. Therefore, in Section 3, in addition to the quantities examined in [2] we examine the entire contour displacement. These contours were reconstructed from the model and experiment data using the nonlinear LIUQE inverse equilibrium reconstruction code [4]. Plasma shape parameters such as κ and δ were also examined. Of particular interest for diverted plasmas were the X-point position and strike point responses. Conclusions are presented in Section 4.

2. PLASMA RESPONSE OF DIRECTLY MEASURED PARAMETERS

2.1 Modelling

The position and shape response of the SND plasma and CREATE-L model were compared in a similar way to that of the previous paper. The linearized model provides the simulated flux and field measurements, which are linearly combined to obtain five control parameters and are used by LIUQE to obtain plasma parameters and shape. These parameters are compared with the experimental ones, once a least square linear fit is removed from both sets of data to get rid of offsets and drifts.

The dynamic evolution of currents flowing in conductors, including coils, passive conductors, and plasma, is described by:

$$d\Psi/dt + \mathbf{R}\, I = V \tag{1}$$

where Ψ is the vector of fluxes linked with each conductor and $\mathbf{R}$ is the resistance matrix. I and V are vectors of conductor currents and applied voltages respectively. Expanding the currents $I(t)$ about their reference values:

$$I(t) = I_{\mathrm{ref}} + \delta I(t) \tag{2}$$

it is possible to obtain the linearized form of (1):

$$\mathbf{L}^{*}\, d(\delta I)/dt + \mathbf{R}\, \delta I = \delta V = \mathbf{B_1}\, \delta U \tag{3}$$

where U is the active coil voltage vector, $\mathbf{B_1}$ is a matrix with appropriate zeros and ones to apply voltages to the PF coils, and $\mathbf{L}^{*} = \partial\Psi/\partial I$ is the modified inductance matrix [3]. The model should be completed by the response to the l_i and β_p variations. However, in the present work, we are only interested to the plasma response to the conductor currents, and therefore neglect these terms.

For control analysis and design purposes, the circuit equations are conveniently cast in a state space form:

$$dx/dt = \mathbf{A}\, x + \mathbf{B}\, u \tag{4}$$

where $\mathbf{A}=-\mathbf{L}^{*-1}\mathbf{R}$, $\mathbf{B}=\mathbf{L}^{*-1}\mathbf{B}_1$, the current $x=\delta I$ is the state vector, and the voltage input $u=\delta U$ is the control vector.

The output variables of main interest are the perturbations of fluxes and fields measured by magnetic sensors, and current moments. With this model, all of them are linear combinations of state variables:

$$y = \mathbf{C}\, x \tag{5}$$

The main differences among the models used in this work mainly reside in the nominal reference configuration and in the treatment of the plasma equation, as is summarised in Table 1. All of the CREATE-L models exclude the presence of skin currents at the plasma boundary, and assume zero plasma resistivity.

The equations used to generate the CREATE-L model were different than those used in [2] for the simplified CREATE-L, but produce essentially the same result. The CREATE-L plasma response model is derived by linearizing the equilibrium equation and Ohm's law in the active and passive conductors and in the plasma. In this model, the plasma is assumed to be in permanent MHD equilibrium and the plasma current density profile is kept fixed, whereas the total plasma current is allowed to vary. The boundary and magnetic axis fluxes are also allowed to vary. The model can be used to predict the plasma current, shape and position response to voltages applied to control coils.

Simulations using the other models introduced in this section test the sensitivity of the plasma model responses to different assumptions on the plasma boundary flux. The RCDM and the plasmaless model are here considered mainly for evaluating the actual importance of the plasma model in the overall response.

The TCV closed loop system is simulated as in Fig. 2 and is described in more detail in [2]. The CREATE-L model of TCV is in state-space form and is represented by the matrices **A**, **B**, **C**, and **D**. The power supplies are modelled as single pole filters with a time constant of 0.3ms. The TCV feedback system comprises a PID controller and feedback matrices $\mathbf{M}$, $\mathbf{K}_1$, and $\mathbf{K}_2$.

2.2 Experiments

The plasma parameters examined in this section are directly measured quantities, obtained from the linear combination of flux loops, poloidal field pickup coils and poloidal field control coil currents. These were the vertical flux imbalance (P_VERT) which provides a measure of radial position; the outboard field curvature (TRI_OUT) and the inboard field curvature (TRI_IN) which together provide a measure of plasma

elongation and triangularity; the vertical position current moment (zI_p); the plasma current (I_p). An additional parameter (ψ_R) was also compared which is related to the radial current moment and is the difference between the R^2I_p current moment and $R_0^2I_p$ where R_0 is the unperturbed major radius. This represents the radial movement contribution to $<R^2j>$. The parameters under feedback control in the experiments were P_VERT, zI_p and I_p. Square pulse stimulation signals were applied to test the response in the time domain. The size and signs of the pulses were chosen to prevent the plasma switching to a limited configuration. The two ohmic heating coils were tested in one discharge. Four of the E coils and four of the F coils were tested in two other discharges, with only one coil excited at any time.

Additional discharges were performed in which RBS signals were applied to three different coils (E1, F1 and F7). Spectral analysis was then used to compare the frequency response from the coils to the measured parameters and the modelled response as in [2].

The experiments produced a variety of responses. The main difference with respect to [2] is that the vertical position and radial positions are coupled. The zI_p response in an up-down asymmetric plasma can no longer be isolated using the up-down antisymmetric stimulation of the previous paper. The excitations provoked peak to peak variations of up to 0.7cm and 3cm in the radial and vertical positions of the plasma axis, and 4kA peak to peak variations in the plasma current. The inboard E coils have a more marked effect on TRI_IN than on TRI_OUT, and the opposite is true for the outboard F coils, and the OH coils have a marked effect on both parameters. Occasional highly oscillatory zI_p responses are also observed when the OH coils are excited, and this will be discussed in detail in Section 3. The use of one coil for stimulation instead of two produces responses with lower signal to noise ratios with respect to [2] and in the frequency domain this leads to "noisy" estimates with wide confidence bounds.

2.3 Model Comparisons

In general the CREATE-L model was found to be in good agreement with the closed loop time and frequency domain responses for all the coils that were tested. The full comparison is presented in Appendix A with the more interesting exceptions and model differences described below. A typical time domain response (Fig. 3) highlights the excellence of the diverted plasma CREATE-L model agreement, which is as good as that for the limited plasma in [2]. The agreement with the plasmaless model is

sometimes reasonable for some control parameters, again also similar to the results in [2]. The TRI_IN response in Fig. 3 is an example of a very close agreement, and the P_VERT response is an example of a poor match. The plasmaless model is clearly of no value for parameters based on current moments.

The time domain closed loop responses between the F coils and TRI_OUT are difficult to distinguish for all the models including the plasmaless model. This is also true in the frequency domain (Fig. 4). The responses are more varied between the E coils and TRI_OUT with a marked difference for the plasmaless model. However the amplitude responses are smaller than for the F coils leading to wider confidence bounds. The link between amplitude and variation between the models also suggests that the closed loop response of TRI_OUT to the F coils is dominated by the vessel, whereas the E coils responses are more influenced by the plasma. Corresponding results for TRI_IN suggests that the E coil responses are dominated by the vessel which is not the case for the F coils.

The frozen flux and asymmetric limited models perform relatively well for all stimulations except for the P_VERT and ψ_R responses. The discrepancy between these two models and the experiment is most visible with OH coil stimulation (Fig. 5). The frozen flux assumption is clearly invalidated in this case, and the ψ_R response is also shown to be sensitive to the shape of the plasma that is modelled. This is understood in terms of changing the assumption of the plasma boundary flux as noted in the Introduction. Small discrepancies between the CREATE-L model and the experimental responses are observed under E and F coil stimulation (Fig. 6, t=0.58s). The frozen flux model is clearly invalidated, but in this case the asymmetric limited plasma model is equally as good as the diverted model. This is also seen in the frequency domain (Fig. 7) above 50Hz.

The P_VERT response is sensitive to the frozen flux assumption and invalidates this model in the same way as the ψ_R responses. However it does not distinguish between the diverted and limited CREATE-L models. All the other non-radial position closed loop responses are insensitive to either assumption and the model-experiment agreement

is always good. The frozen flux model radial position responses are always much more underdamped than the experiment when I_p is changing rapidly.

2.3.1 Vertical position

The most striking feature of the experimental data is the oscillations in zI_p which occur when the OH coils are stimulated (Fig. 8). This feature is investigated in detail because of the importance of the vertical instability to the control system performance. The response is highly resonant between 0.42s and 0.5s with an oscillation frequency of 138Hz. None of the linear models is able to reproduce the oscillations but they all successfully predict the non oscillatory component of the step response. Therefore the occurrence and subsequent disappearance of the oscillations must be attributed to nonlinear and/or time varying features of the system.

In fact the oscillations can be linked to changes in the open loop vertical instability growth rate over time. The growth rate depends on the ratio of the "stabilizing" force (F_s) and the "destabilizing" force (F_d) due to an instantaneous vertical displacement (δz) as well as the vessel resistance. In the context of the RCDM [1], the destabilizing force is due to the equilibrium quadrupole field required for vertically elongated plasmas and it is assumed that no initial vessel currents contribute,

$$F_d = \delta z \int j(\boldsymbol{r}) \frac{\partial (\boldsymbol{B}_{\mathbf{Ra}}^{\mathrm{T}}(\boldsymbol{r}) \boldsymbol{I}_{\mathbf{a}})}{\partial z} d^3\boldsymbol{r} \qquad (6)$$

where $\boldsymbol{I}_{\mathbf{a}}$ is the vector of active coil currents, each element of $\boldsymbol{B}_{\mathbf{Ra}}(\boldsymbol{r})$ is the radial field produced by a unit current in the corresponding element of $\boldsymbol{I}_{\mathbf{a}}$, and $j(\boldsymbol{r})$ is the plasma current density. As the plasma moves away from its equilibrium position the radial component of the shaping field acts to push the plasma further away. The plasma displacement induces image currents in the surrounding passive vessel structure given by the amplitudes of their eigenvectors,

$$\boldsymbol{I}_{\mathbf{v}} = \mathbf{L}_{\mathbf{v}}^{-1} \delta z \int j(\boldsymbol{r}) \boldsymbol{B}_{\mathbf{Rv}}(\boldsymbol{r}) d^3\boldsymbol{r} \qquad (7)$$

where the elements of $\boldsymbol{I}_{\mathbf{v}}$ are the vessel eigenmode currents, $\boldsymbol{B}_{\mathbf{Rv}}(\boldsymbol{r})$ is the vector of radial fields produced by a unit current in each eigenmode and $\mathbf{L}_{\mathbf{v}}$ is the diagonal mutual inductance matrix of the eigenmodes (thereby correcting the erroneous Eq. (6) of [1]). Since the vessel is poloidally and toroidally continuous, the initial flux change outside

the vessel is zero and therefore currents induced in structures outside the vessel can be neglected. The vessel image currents set up fields providing a stabilizing force acting to oppose the plasma displacement,

$$F_s = \int j(\boldsymbol{r})\boldsymbol{B}_{\mathrm{Rv}}^{\mathrm{T}}(\boldsymbol{r})\boldsymbol{I}_{\mathrm{v}}d^3\boldsymbol{r} \qquad (8)$$

The RCDM model was used to calculate the force gradients and growth rates at 10ms time intervals throughout the OH stimulation shot (Fig. 9). The growth rate varies from 50 s^{-1} when the plasma is damped to over 350 s^{-1} when the response is oscillatory. The effect of plasma current changes on the growth rate has been calculated as in [5]. For the worst case current ramp the growth rate varies by less than 10 s^{-1} and so the effect has been neglected here.

As the gross plasma position changes, the vertical gradient of the radial field ($\partial B_R/\partial z$) averaged over the plasma current distribution varies and the destabilizing force changes. If the coil currents are fixed then $\partial B_R/\partial z$ is fairly uniform over the range of plasma radial movement (±3mm). The variation in $\partial B_R/\partial z$ is dominated by any changes to the coil currents. The contribution from vessel currents, calculated using flux loops around the vessel, contribute less than 3% of the $\partial B_R/\partial z$ field. As the plasma moves, the feedback controller alters the coil currents in response, changing the poloidal field such that both the plasma elongation and the growth rate vary. The coupling to the vessel, and hence the stabilizing force, also changes but the effect is less marked. The changes in F_s and F_d are around 15% but the effect on the growth rate is noticeable because of the small plasma stability margin. The system remains locally linearizable around a working point but should the working point change beyond the region of validity of the model, the differences between plasma and model responses become noticeable.

High open loop instability growth rates lead to a more resonant closed loop response (Fig. 10). A resonant peak is predicted by the closed loop RCDM model at 130Hz for the plasma equilibrium at time 0.47s. Oscillations occur at this time with frequency 120Hz (Fig. 8). A damped response is predicted for the plasma equilibrium at time 0.62s and the experiment confirms that no oscillations are observed. The coupling between the plasma position and the growth rate is observed to a lesser extent in the E

and F coil stimulation shots. The variation in growth rate is between 100 and 250 s^{-1}. The peak growth rate is enough to cause underdamped zI_p responses but not as resonant as in the OH shot (Fig. 11). The same relationship between the closed loop damping factor and the open loop growth rate is observed.

The CREATE-L models closely match the experimental result. This is due to the similar open loop instability growth rates between the CREATE-L model (223 s^{-1}) and the frozen flux model (268 s^{-1}) both of which were calculated for the plasma equilibrium at 0.35s, the asymmetric limited model (236 s^{-1}) and the RCDM model (264 s^{-1}). The models with the higher growth rates have more resonant closed loop responses, with the resonant frequencies around 115 Hz. The modelled growth rates for the plasma at 0.46s is 434 s^{-1} for the shifted CREATE-L model and 508 s^{-1} for the shifted frozen flux model. The level of underdamping also depends on the power supply time constant. This was chosen in [2] as 0.3ms for the CREATE-L model. No doubt any of the other model responses could have been made to agree more closely had the time constant been tuned on the relevant model. For example, for the RCDM model changing the power supply time constant to 0.7s leads to an agreement as accurate as that for the CREATE-L model and 0.3ms power supplies.

The coupling existed in the symmetric stimulation discharges of the up-down symmetric limited plasma in [2], but this effect was not examined because symmetric stimulation of a symmetric plasma does not excite zI_p. The change in growth rate is definitely more strongly coupled to radial position than vertical position because the effect was not observed for antisymmetric stimulation of zI_p in [2].

3. PLASMA RESPONSE OF RECONSTRUCTED EQUILIBRIUM PARAMETERS

The introduction of a separatrix allows us to question the modelling of the plasma contour shape and position. The movement of the separatrix determines the wall contact and the divertor geometry. The separatrix position is perhaps of more interest than feedback control parameters because its physical interpretation is more immediate and it is proposed that this be controlled directly on ITER. On TCV the separatrix position and shape is reconstructed from the magnetic pick-up signals and poloidal field coil currents

using the LIUQE code [4]. This code has been used to reconstruct the separatrix movement from the simulated data as well as the experimental data and a comparison is presented in this Section.

The evolution of many reconstructed plasma parameters was examined. For all coil stimulations the experimental and simulated traces are consistent to within the resolution of the LIUQE program (Fig. 12). The exception is for oscillations in the magnetic axis vertical position which occur at around 0.45 s seen clearly when the OH coils are excited, and to a lesser extent in the vertical position of the X-point. The separatrix parameters examined included the positions of the X-point which varied between 0.625 to 0.652 m radially and -0.246 to -0.23 m vertically, the plasma strike points (±4 cm), and the minimum (0.626 to 0.639 m) and maximum (1.108 to 1.118 m) radial points on the plasma. Shape parameters at the 95% flux surface such as the elongation (1.35 to 1.45) and the upper (0.05 to 0.11) and lower (0.39 to 0.45) triangularity were also in good agreement. Other parameters included the position of the magnetic axis (0.885 to 0.892 m radially and 0.110 to 0.136 m vertically) and the safety factor (4.0 to 4.5) at the 95% flux surface. More details are provided in Appendix A.

The evolution of 12 minor radii at equal poloidal angles around the plasma was also calculated. They were defined to be the distances from the experimental plasma magnetic axis to the plasma last closed flux surface of either the experimental or the simulated data. The minor radii of the plasma are plotted in Fig. 13. The first radius, labelled 'gap 1', points horizontally out away from the centre column and the other radii are spaced at 30 degrees anticlockwise around the plasma. Hence the traces labelled 'gap 4' and 'gap 10' represent the distance to the top and the bottom of the plasma respectively. The traces agree to within the accuracy of the reconstruction except for the plasma vertical position oscillation.

4. DISCUSSION

The plasma responses of an up-down asymmetric SND TCV plasma are modelled accurately by the CREATE-L plasma model. This extends our previous work which was restricted to limited and centred plasmas. The only exception to the almost perfect agreement is the appearance of zI_p oscillations. This occurs when the test stimulation is such that the growth rate is significantly modified, removing the linearity of the experimental responses and hence disallowing the use of a time-invariant linear model. This highlights the nonlinear nature of the system with implications for controller design. Linear models are still valid if regulation around an equilibrium point is

specified. However tracking over a large parameter space would require assessment of any variations of the linearized model.

Extension to an SND plasma has also allowed us to test the modelling of the displacement of the separatrix contour, which is found to be in good agreement with the experimental results. In addition to the closed flux surface, the movement of the open divertor strike points is well modelled.

Some of the responses of the closed loop are found to be particularly sensitive to the physics assumptions underlying the CREATE-L linearization. This has allowed us to validate or invalidate the physics content of the plasma response model compared with the purely engineering content of the coil positions and vessel structure. The plasma asymmetry and the possibility of surface currents have not invalidated the assumptions, at least for an Ohmic current profile. An alternative assumption of frozen flux at the plasma boundary has frequently been proposed. This assumption is clearly invalidated by the radial movement of the plasma. The ψ_R parameter is seen to be a sensitive indicator of model validity. This is apparent when an asymmetric limited plasma model is compared to the diverted experiments.

The closed loop response of the CREATE-L model has not been found to be invalidated by any of the experimental data. This allows increased confidence in its use for controller design purposes but still cannot be considered as qualified for this purpose. Qualified in this sense implies that the performance of any controller designed with this model would be achieved when used. Work is in progress to qualify the open loop response of the model on TCV.

ACKNOWLEDGEMENTS

Useful discussions with Profs. G. Rubinacci and G. Ambrosino of the CREATE team and Drs. F. Hofmann and R.A. Pitts of the TCV team are gratefully acknowledged. The TCV team are also thanked for their contributions to the experiments. This work was partly supported by a EURATOM mobility contract (FV) and partly by the Fonds national suisse de la recherche scientifique.

REFERENCES

[1] LISTER, J.B., MARTIN, Y., MORET, J.-M., Nuclear Fusion **36** (1996) 1547.
[2] VILLONE, F., VYAS, P., LISTER, J.B., ALBANESE, R., accepted for publication in Nuclear Fusion (1997);

VILLONE, F., VYAS, P., LISTER, J.B., ALBANESE, R., "Comparison of the CREATE-L Plasma Response Model with TCV Limited Discharges," Report LRP 569/97, CRPP, Lausanne (1997).
[3] ALBANESE, R., VILLONE, F., "The Linearized CREATE-L Plasma Response Model for the Control of Current, Position and Shape in Tokamaks," submitted to Nuclear Fusion (1997).
[4] HOFMANN, F., TONETTI, G., Nuclear Fusion **28** (1988) 1871.
[5] LAZARUS, E.A., LISTER, J.B., NEILSON, G.H., "Control of the Vertical Instability in Tokamaks," Nuclear Fusion **30** (1990) 111

TABLES

Table 1
Basic assumptions for the derivation of the various models of TCV plasmas (#12610)

	derivation approach	*plasma current response to conductor currents*	*flux at the plasma boundary*	*reference configuration*
CREATE-L	perturbed equilibrium	linearization of $\int \boldsymbol{E}\cdot\boldsymbol{J}dV = \int \boldsymbol{v}\cdot\nabla p dV$	given by the flux at the reference X-point location	nominal diverted configuration at t=0.3 s
simplified CREATE-L	perturbed equilibrium	linearization of $\int E_{tor}\cdot J_{tor}dV = 0$	given by the flux at the reference X-point location	nominal diverted configuration at t=0.3 s
limited CREATE-L	perturbed equilibrium	linearization of $\int \boldsymbol{E}\cdot\boldsymbol{J}dV = \int \boldsymbol{v}\cdot\nabla p dV$	given by the flux at the reference plasma-wall contact point	modified limited shape of Fig. 1
frozen flux CREATE-L	perturbed equilibrium	linearization of $\int \boldsymbol{E}\cdot\boldsymbol{J}dV = \int \boldsymbol{v}\cdot\nabla p dV$	frozen	nominal diverted configuration at t=0.3 s
shifted CREATE-L	perturbed equilibrium	linearization of $\int \boldsymbol{E}\cdot\boldsymbol{J}dV = \int \boldsymbol{v}\cdot\nabla p dV$	given by the flux at the reference X-point location	diverted configuration - radial shift, t=0.46 s
shifted frozen flux CREATE-L	perturbed equilibrium	linearization of $\int \boldsymbol{E}\cdot\boldsymbol{J}dV = \int \boldsymbol{v}\cdot\nabla p dV$	frozen	diverted configuration - radial shift, t=0.46 s
RCDM	rigid current displacement	conservation of I_p	———	I_p = 200 kA
plasmaless	pure electromagnetic analysis	———	———	———

FIGURES

Fig. 1. TCV tokamak with diverted (solid) and limited (dashed) plasma shapes. The poloidal field coils are labelled 'E1' to 'E8' on the inboard side, 'F1' to 'F8' on the outboard side and the two ohmic coil sets are labelled 'OH1' and 'OH2'. Poloidal field probes are marked '-' inside the tiles and flux loops are marked 'x'.

Fig. 2. Schematic diagram of the TCV feedback control system.

Fig. 3. Experimental (light solid), CREATE-L (dark solid), and plasmaless model (dashed) responses to E coil stimulation.

Fig. 4. Experimental and modelled TRI_OUT frequency responses to F1 coil stimulation. Experimental response (light solid) with confidence bounds (light dashed), CREATE-L (dark solid), plasmaless (dark dashed); frozen flux CREATE-L and limited CREATE-L responses are indistinguishable from the CREATE-L response.

Fig. 5. Experimental (light solid), CREATE-L (dark solid), frozen flux CREATE-L (dotted) and limited CREATE-L (dashed) ψ_R responses to OH coil stimulation.

Fig. 6. Experimental (light solid), CREATE-L (dark solid), frozen flux CREATE-L (dotted) and limited CREATE-L (dashed) ψ_R responses to E coil stimulation.

Fig. 7. Experimental and modelled ψ_R frequency responses to E1 coil stimulation. Experimental response (light solid) with confidence bounds (light dashed), CREATE-L (dark solid), frozen flux CREATE-L (dark dotted) and limited CREATE-L (dark dashed).

Fig. 8. Experimental (light) and CREATE-L (dark) zI_p responses to OH coil stimulation.

Fig. 9. Plasma response to OH coil stimulation with the radial position of the magnetic axis (R_{axis}), the plasma vertical position instability growth rate (γ), the stabilizing force gradient ($F_s/\delta z$) and the destabilizing force gradient ($F_d/\delta z$).

Fig. 10. Closed loop zI_p frequency responses calculated from RCDM models for resonant system (solid, #12610, t=0.47 s) and damped system (dashed, #12610, t=0.62 s)

Fig. 11. Experimental (light solid) and CREATE-L (dark solid) zI_p responses to F coil stimulation.

Fig. 12. Reconstructed plasma shape and position parameters showing safety factor (q), elongation (κ) and upper triangularity (δ) at the 95% flux surface, and plasma magnetic axis vertical position (z_{axis}) and the radial and vertical position of the X-point.

Fig. 13. Reconstructed plasma minor radii.

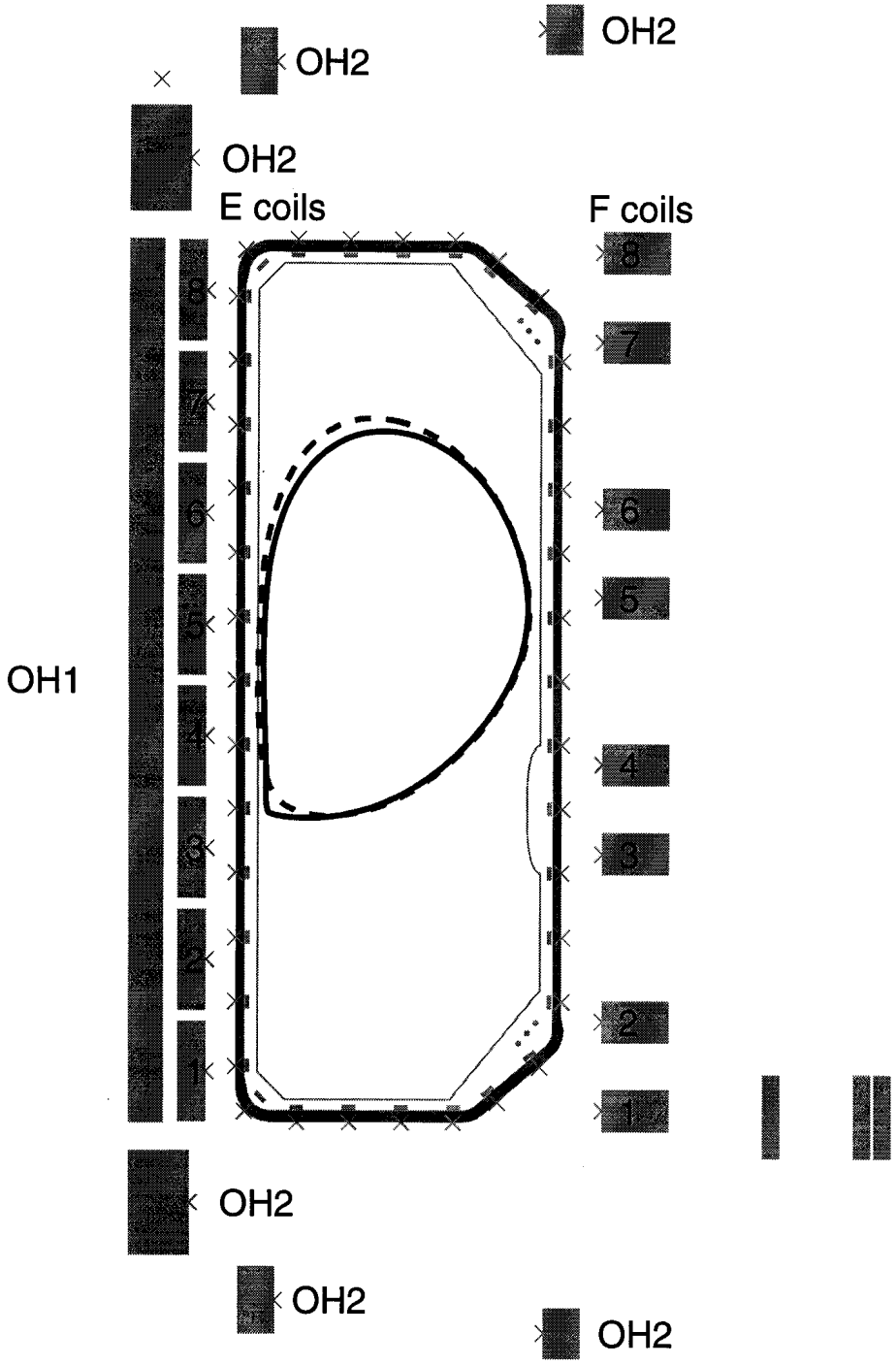

Fig. 1. TCV tokamak with diverted (solid) and limited (dashed) plasma shapes. The poloidal field coils are labelled 'E1' to 'E8' on the inboard side, 'F1' to 'F8' on the outboard side and the two ohmic coil sets are labelled 'OH1' and 'OH2'. Poloidal field probes are marked '-' inside the tiles and flux loops are marked 'x'.

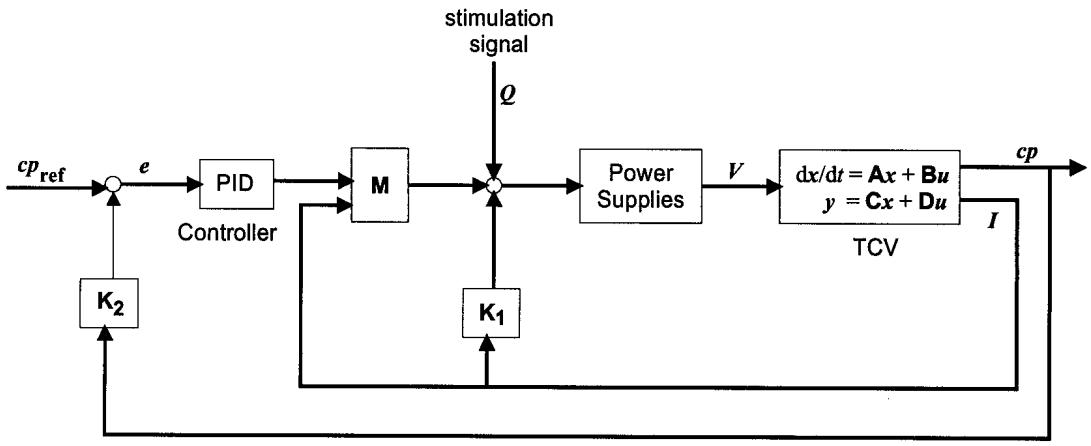

Fig. 2. Schematic diagram of closed loop control system.

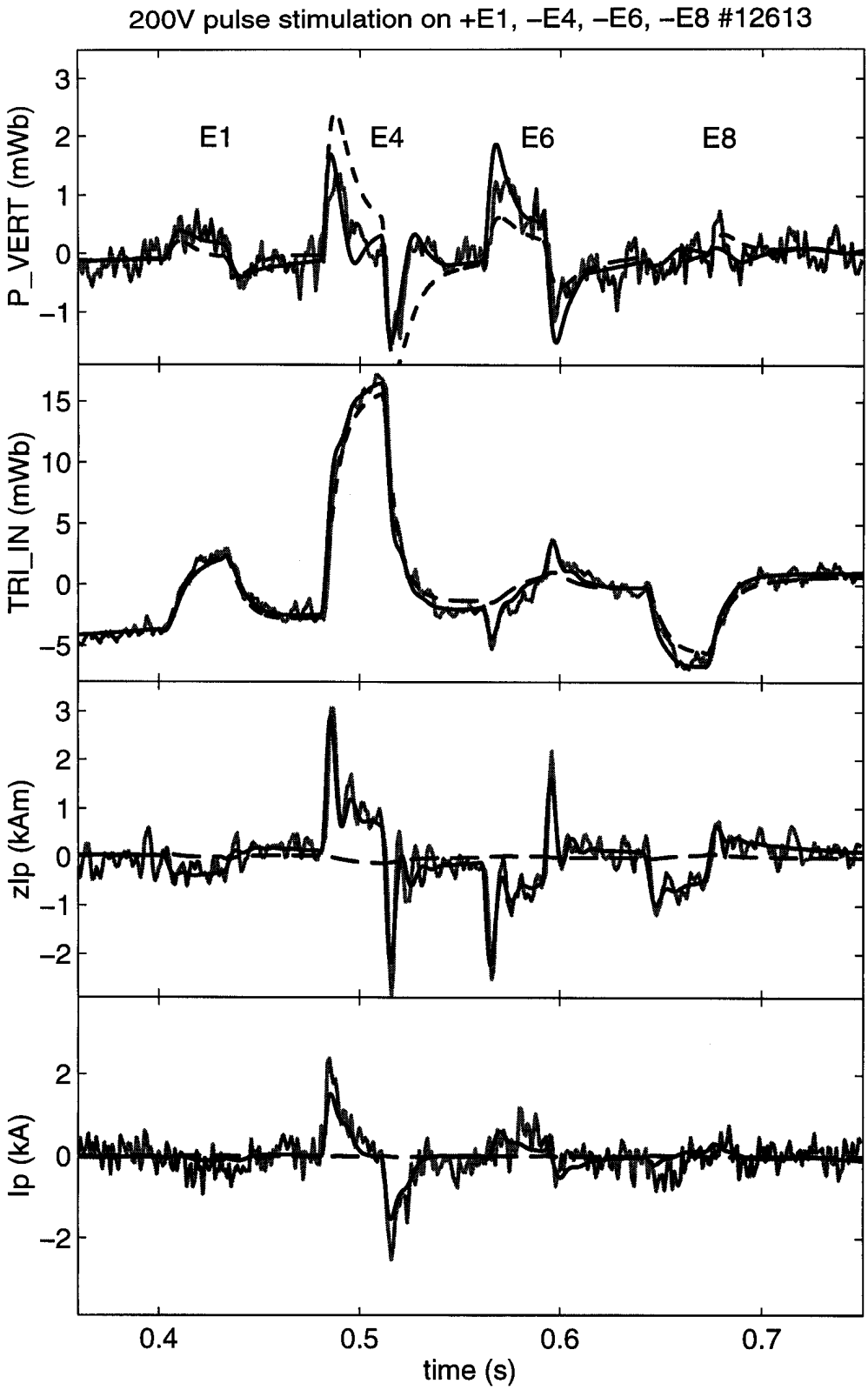

Fig. 3. Experimental (light solid), CREATE-L (dark solid), and plasmaless model (dashed) responses to E coil stimulation.

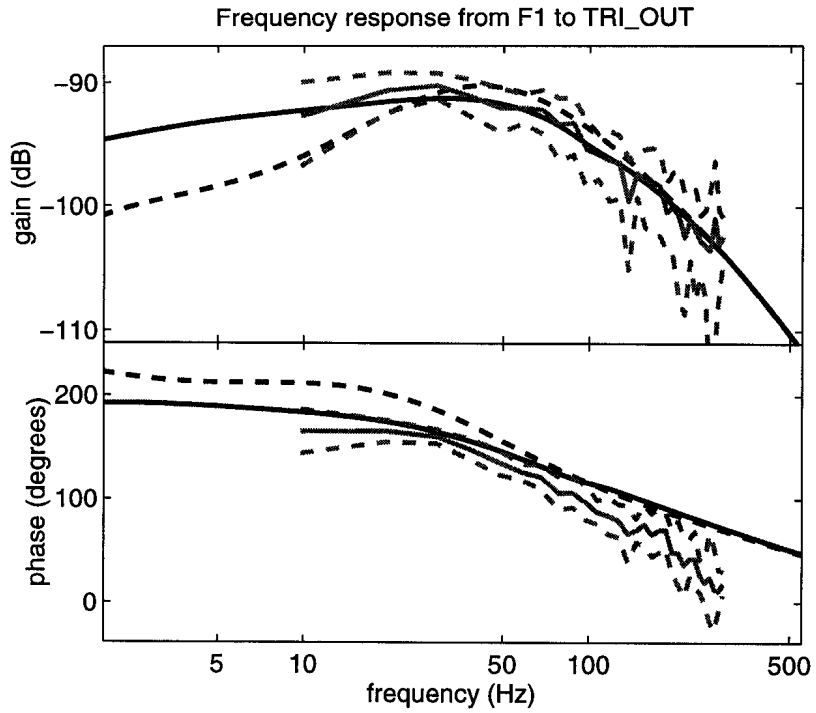

Fig. 4. Experimental and modelled TRI_OUT frequency responses to F1 coil stimulation. Experimental response (light solid) with confidence bounds (light dashed), CREATE-L (dark solid), plasmaless (dark dashed); frozen flux CREATE-L and limited CREATE-L responses are indistinguishable from the CREATE-L response.

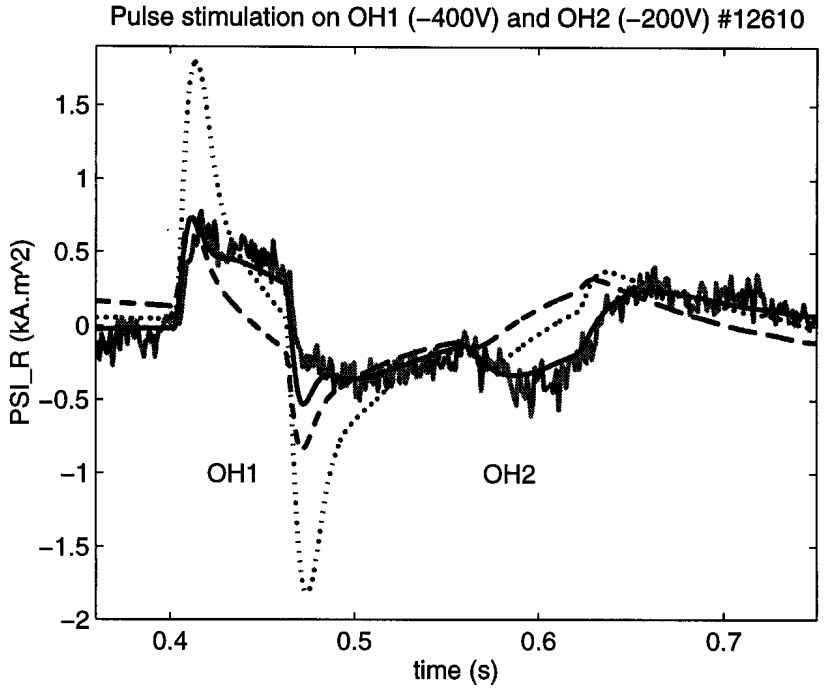

Fig. 5. Experimental (light solid), CREATE-L (dark solid), frozen flux CREATE-L (dotted) and limited CREATE-L (dashed) ψ_R responses to OH coil stimulation.

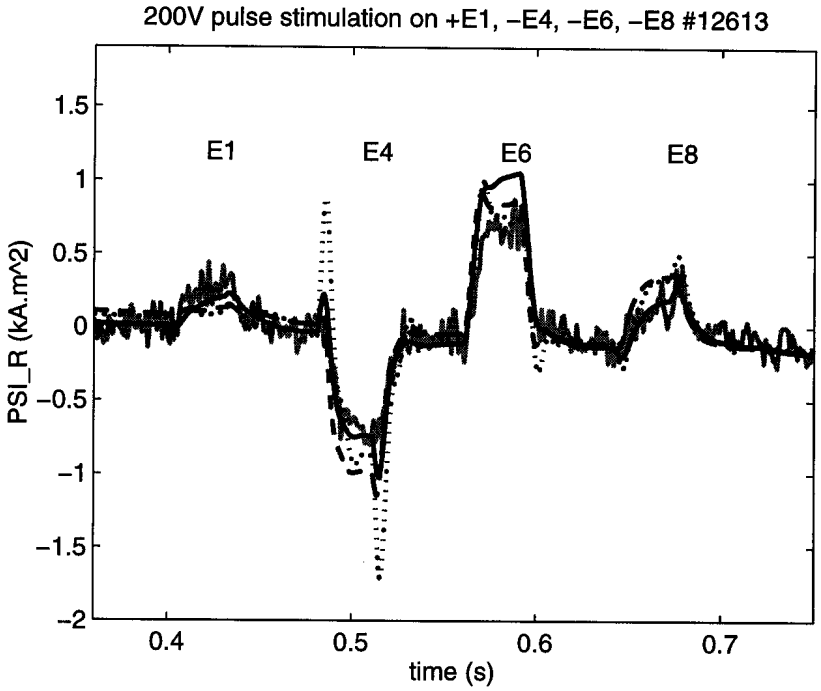

Fig. 6. Experimental (light solid), CREATE-L (dark solid), frozen flux CREATE-L (dotted) and limited CREATE-L (dashed) ψ_R responses to E coil stimulation.

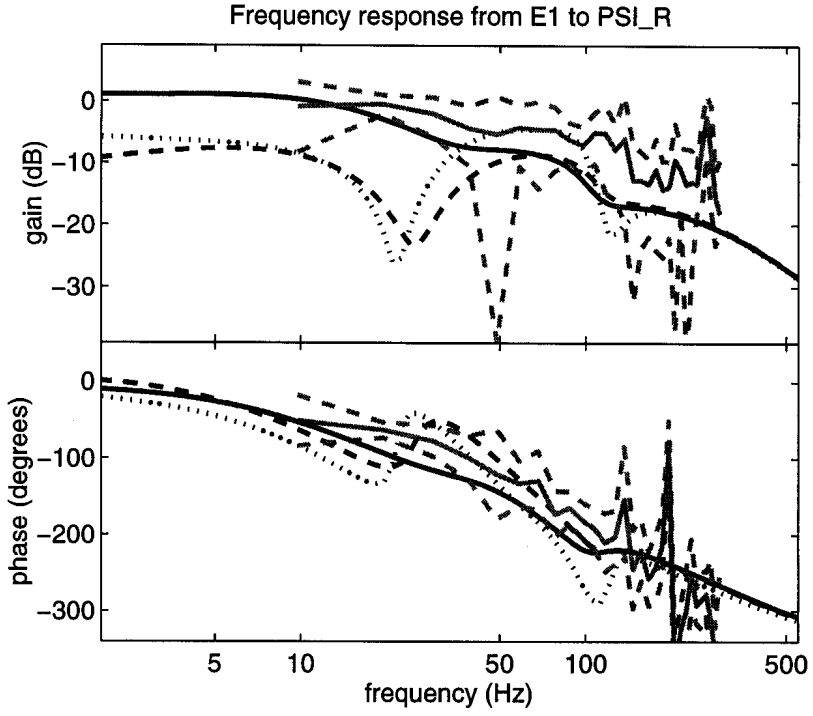

Fig. 7. Experimental and modelled ψ_R frequency responses to E1 coil stimulation. Experimental response (light solid) with confidence bounds (light dashed), CREATE-L (dark solid), frozen flux CREATE-L (dark dotted) and limited CREATE-L (dark dashed).

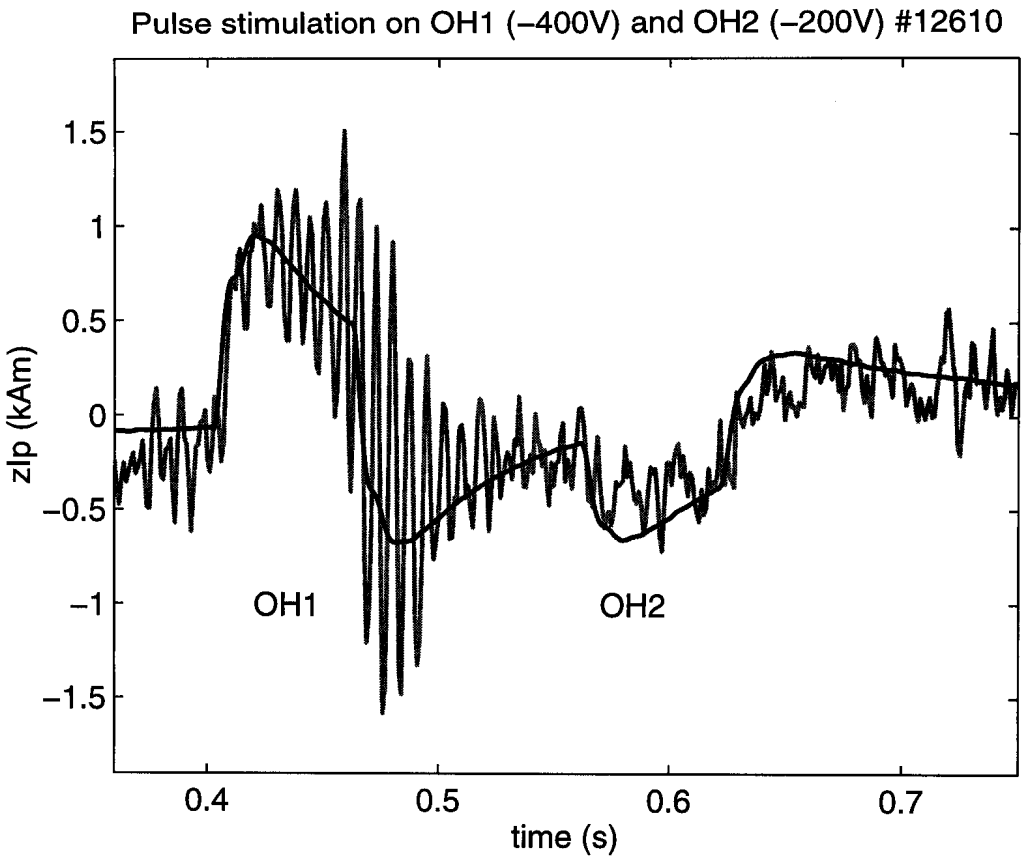

Fig. 8. Experimental (light) and CREATE-L (dark) zI_p responses to OH coil stimulation.

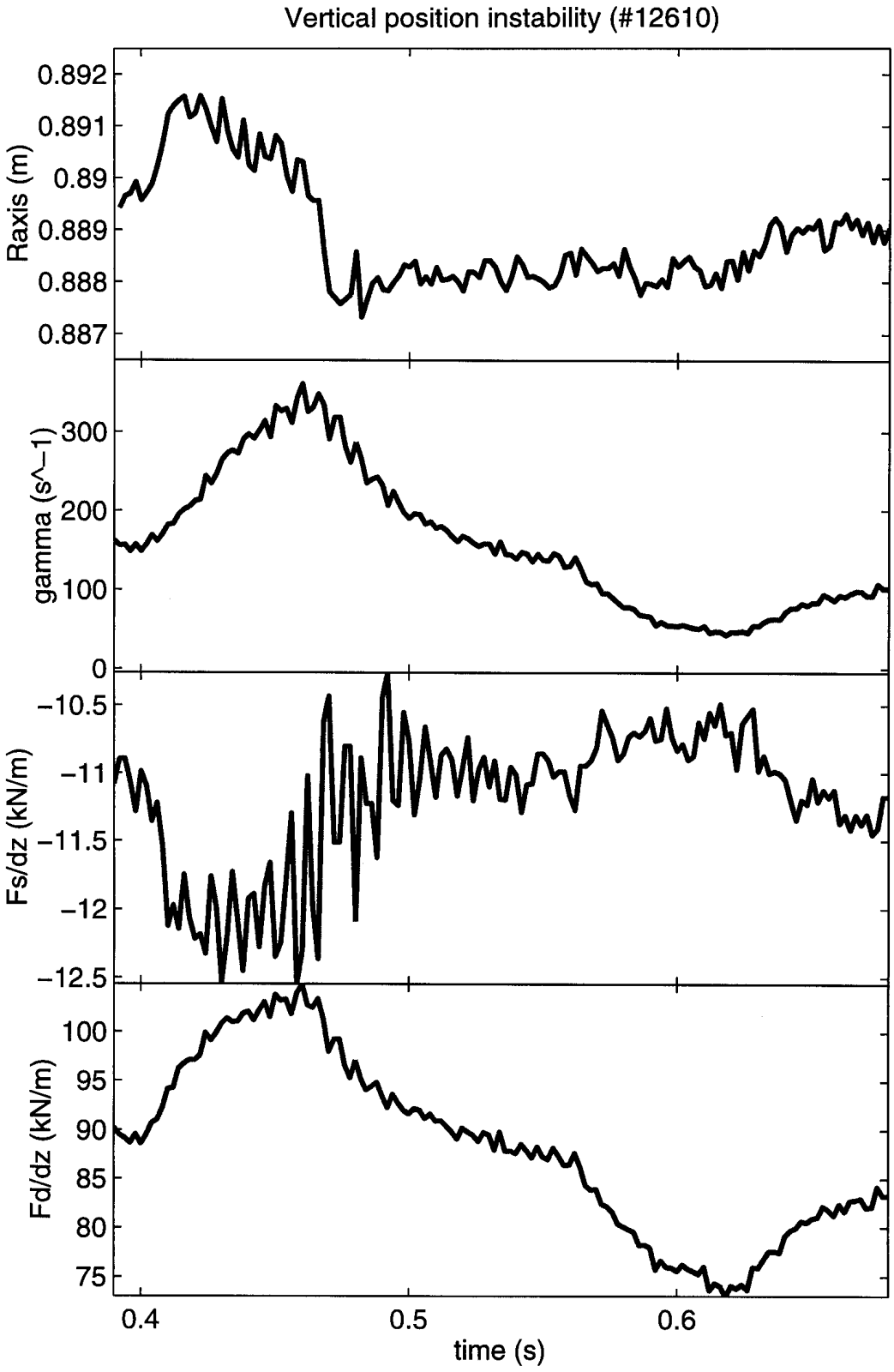

Fig. 9. Plasma response to OH coil stimulation with the radial position of the magnetic axis (R_{axis}), the plasma vertical position instability growth rate (γ), the stabilizing force gradient ($F_s/\delta z$) and the destabilizing force gradient ($F_d/\delta z$).

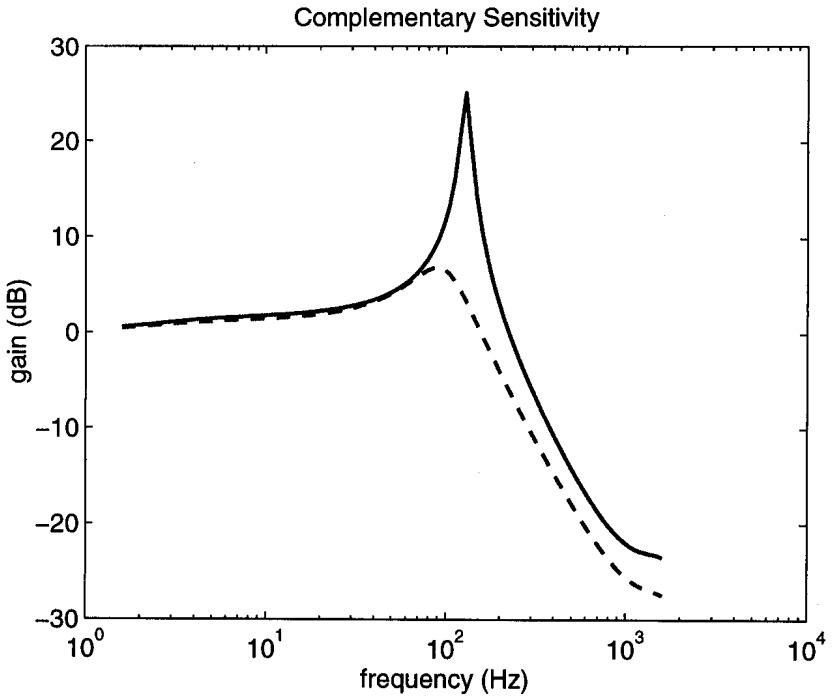

Fig. 10. Closed loop zI_p frequency responses calculated from RCDM models for resonant system (solid, #12610, t=0.47 s) and damped system (dashed, #12610, t=0.62 s)

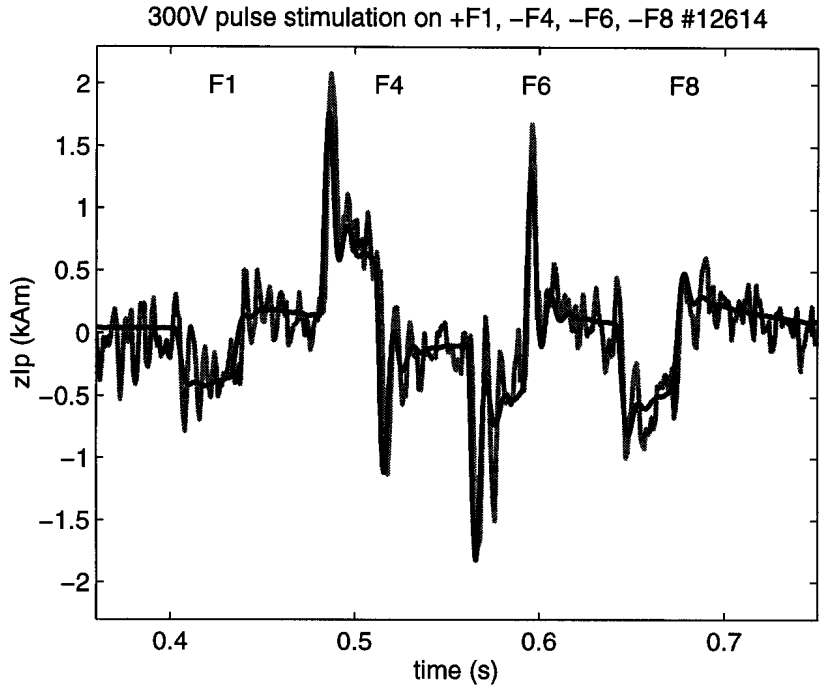

Fig. 11. Experimental (light solid) and CREATE-L (dark solid) zI_p responses to F coil stimulation.

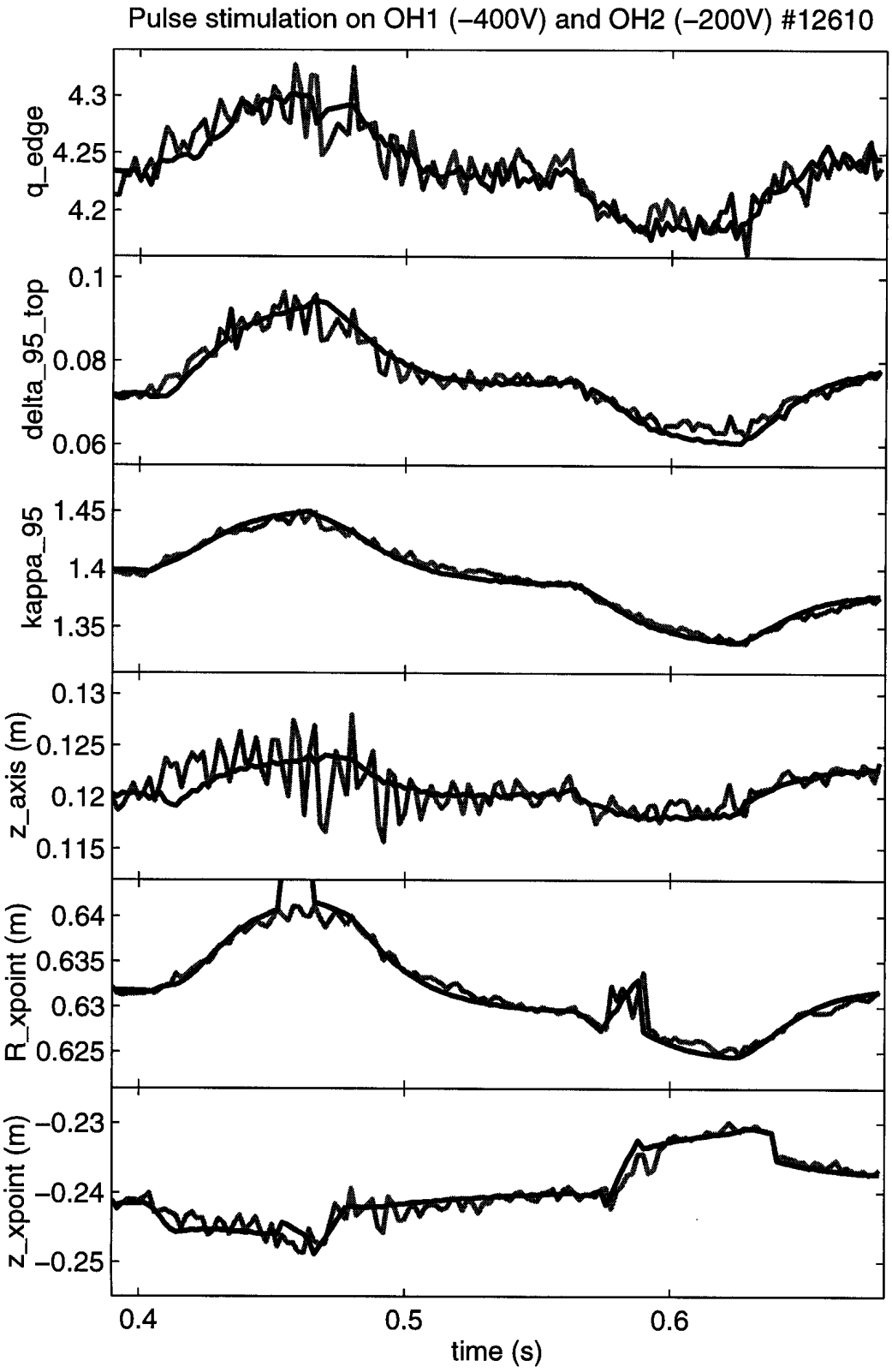

Fig. 12. Reconstructed plasma shape and position parameters showing safety factor (q), elongation (κ) and upper triangularity (δ) at the 95% flux surface, and plasma magnetic axis vertical position (z_{axis}) and the radial and vertical position of the X-point.

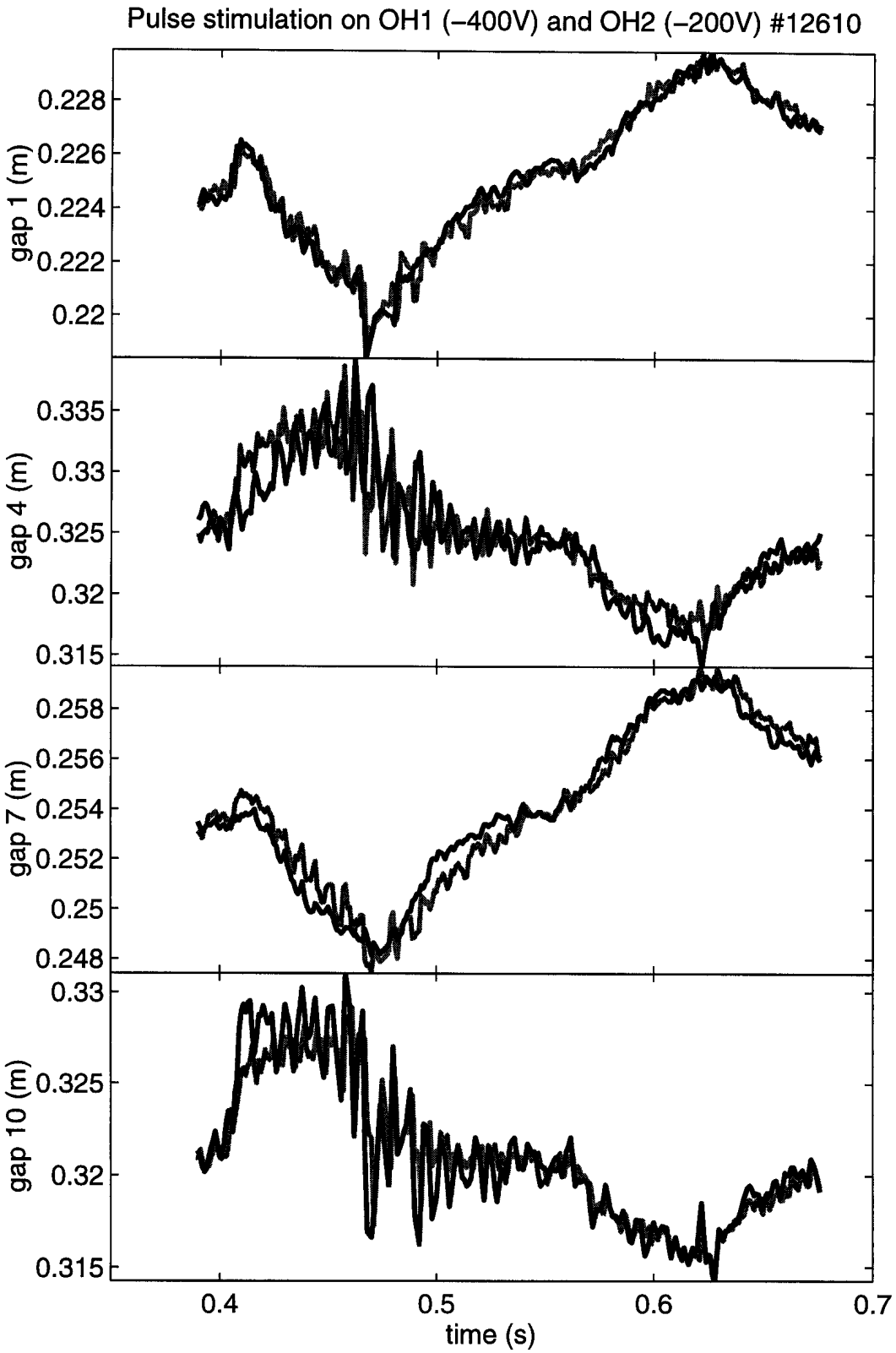

Fig. 13. Reconstructed plasma minor radii.

APPENDIX A

This Appendix records a more complete comparison between the CREATE-L and experimental plasma response. The results are a confirmation of the above Sections and are summarized below.

Stimulation using an RBS signal was applied to coils E1, F1 and F7 and this data was used to derive the experimental closed loop frequency responses in (Figs. A1 to A6). The experimental and CREATE-L responses are always similar, except when the error bounds of the estimates are large. The model-experiment agreement is particularly evident when there are noticeable differences between the coil responses such as for the TRI_OUT parameter in Fig. A2.

The control parameter time domain responses in Figs. A7 to A12 confirm that there are no other model-experiment discrepancies other than those observed in Sections 2 and 3. The agreement with the CREATE-L model is excellent, except for oscillations observed in zI_p and small discrepancies in ψ_R as already noted (Figs. A7 to A9). The frozen flux and limited models are clearly invalidated (Figs. A10 to A12) especially by the ψ_R signal.

Reconstructed plasma shape and position parameters (Figs. A13 to A18) show that the CREATE-L models agrees well with the experimental data. The shape and position of the plasma, along with the magnetic axis and X-point positions were all calculated using the LIUQE inverse equilibrium reconstruction code. The plasma has two strike points on the inboard side of the vessel. The vertical positions of the strike points were calculated from LIUQE derived flux surfaces and are also plotted where possible. The model-experiment agreement is always good.

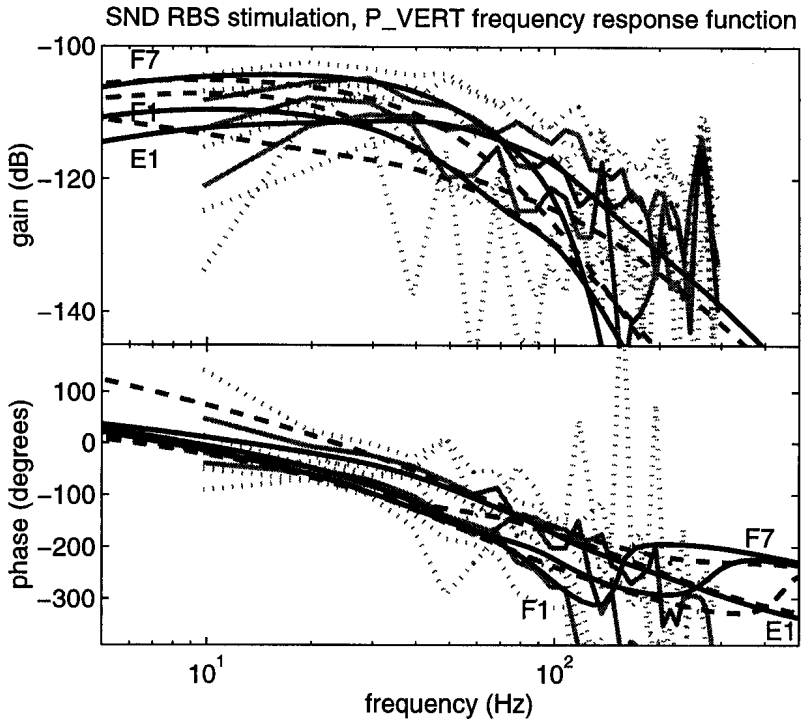

Fig. A1. Comparison of the experimental, CREATE-L and plasmaless CREATE-L frequency responses of P_VERT to RBS stimulation. Experimental spectral analysis estimate (light solid) with associated +/- 3 standard deviation bounds (dotted), CREATE-L model (dark solid) and plasmaless model (dashed).

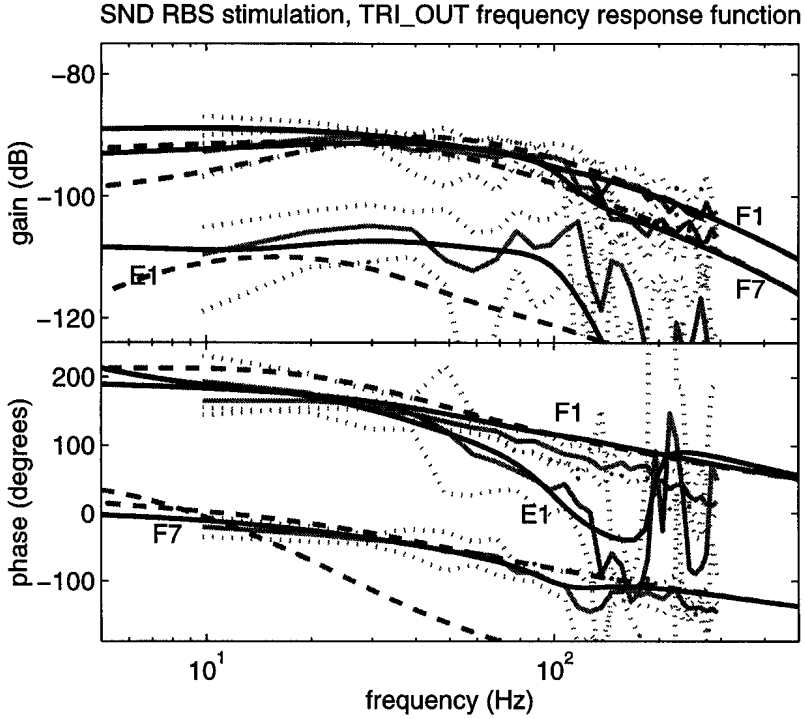

Fig. A2. Comparison of the experimental, CREATE-L and plasmaless CREATE-L frequency responses of TRI_OUT to RBS stimulation. Experimental spectral analysis estimate (light solid) with associated +/- 3 standard deviation bounds (dotted), CREATE-L model (dark solid) and plasmaless model (dashed).

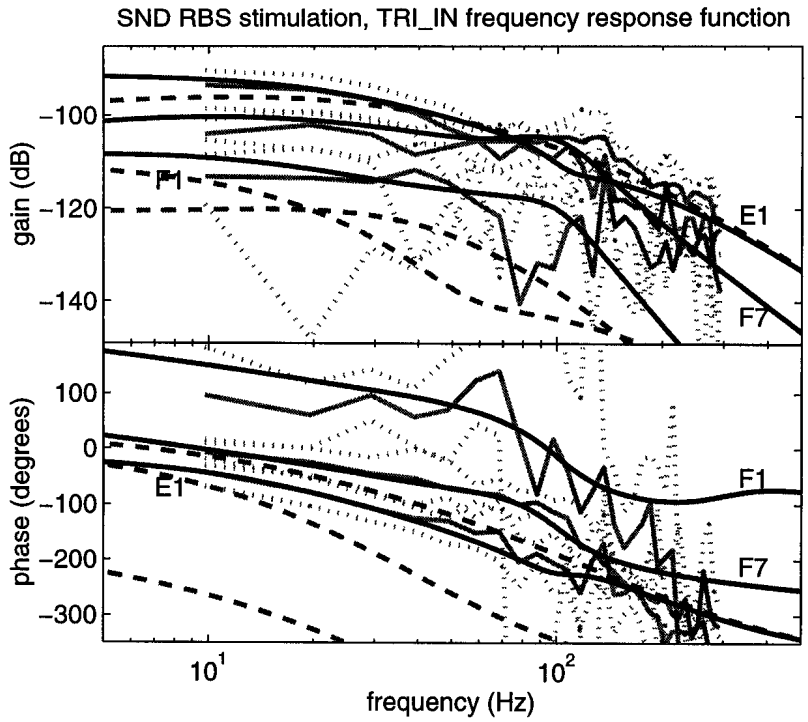

Fig. A3. Comparison of the experimental, CREATE-L and plasmaless CREATE-L frequency responses of TRI_IN to RBS stimulation. Experimental spectral analysis estimate (light solid) with associated +/- 3 standard deviation bounds (dotted), CREATE-L model (dark solid) and plasmaless model (dashed).

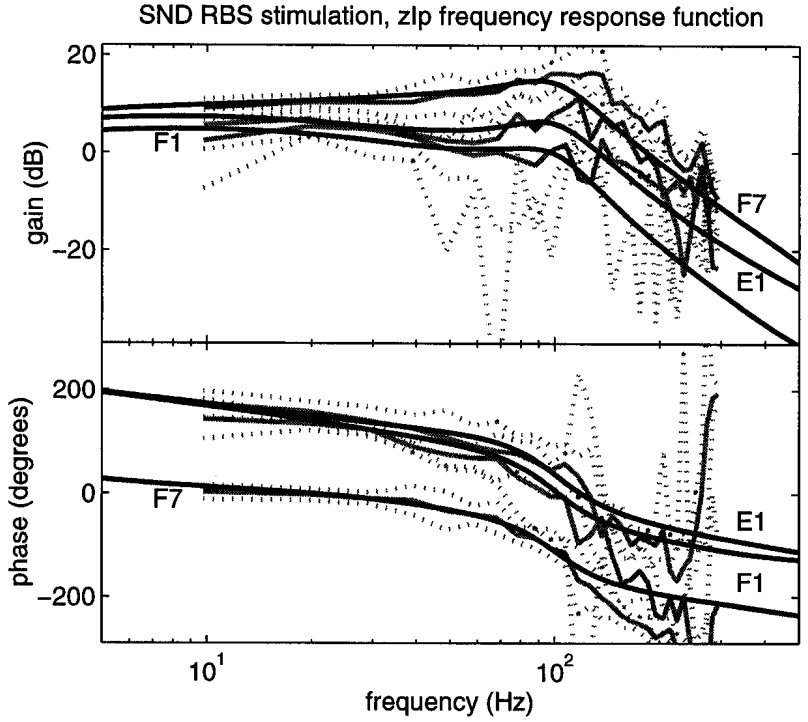

Fig. A4. Comparison of the experimental and CREATE-L frequency responses of zI_p to RBS stimulation. Experimental spectral analysis estimate (light solid) with associated +/- 3 standard deviation bounds (dotted) and CREATE-L model (dark solid).

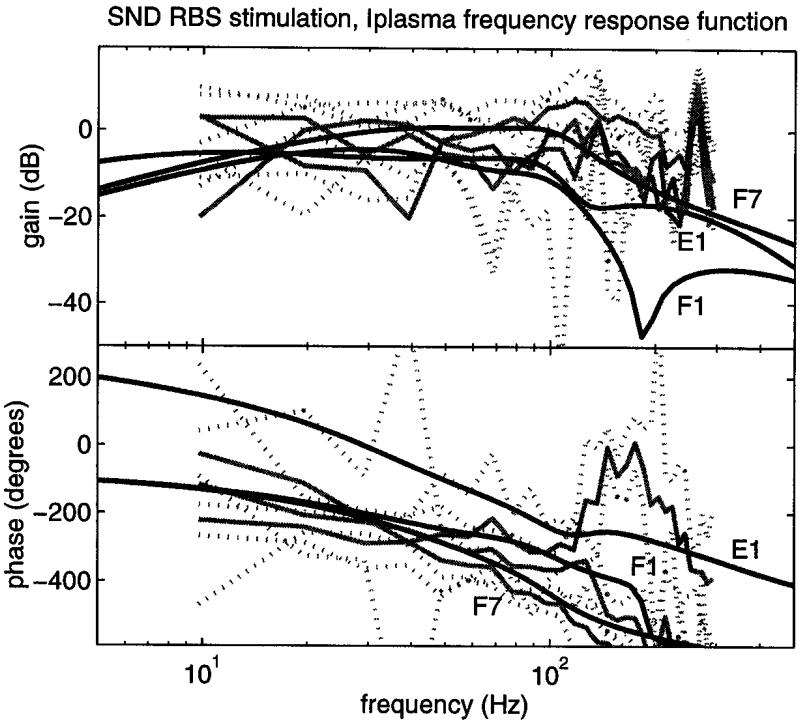

Fig. A5. Comparison of the experimental and CREATE-L frequency responses of I_p to RBS stimulation. Experimental spectral analysis estimate (light solid) with associated +/- 3 standard deviation bounds (dotted) and CREATE-L model (dark solid).

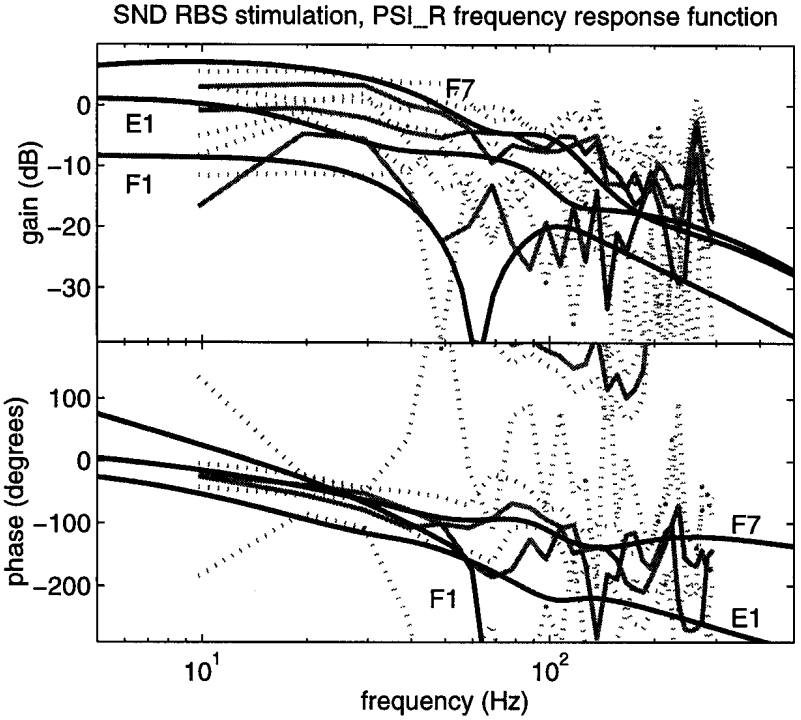

Fig. A6. Comparison of the experimental and CREATE-L frequency responses of ψ_R to RBS stimulation. Experimental spectral analysis estimate (light solid) with associated +/- 3 standard deviation bounds (dotted) and CREATE-L model (dark solid).

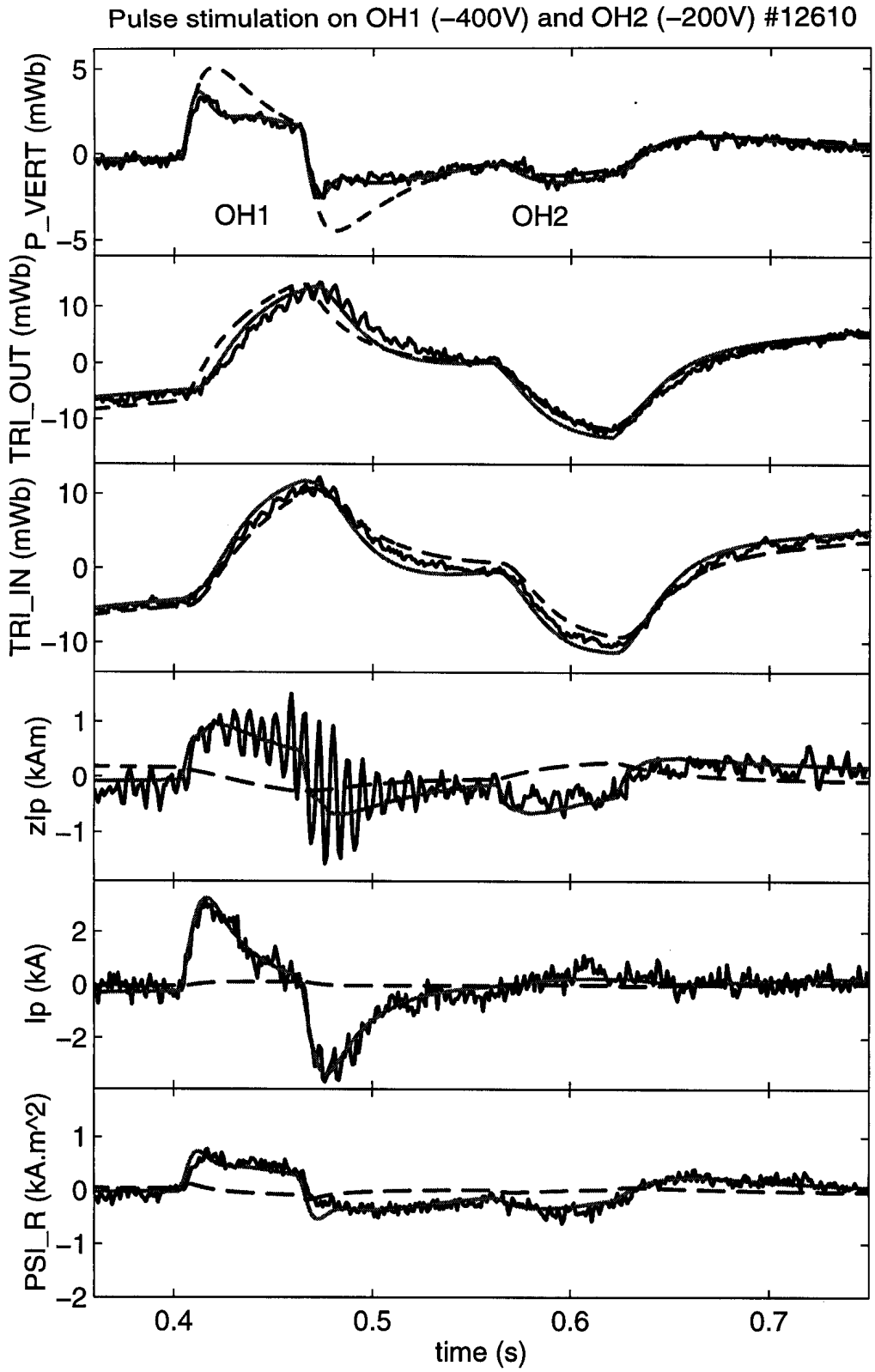

Fig. A7. Comparison of the experimental, CREATE-L and plasmaless CREATE-L responses to square pulse stimulation on the OH coils. Experimental response (dark solid), CREATE-L (light), plasmaless CREATE-L (dashed).

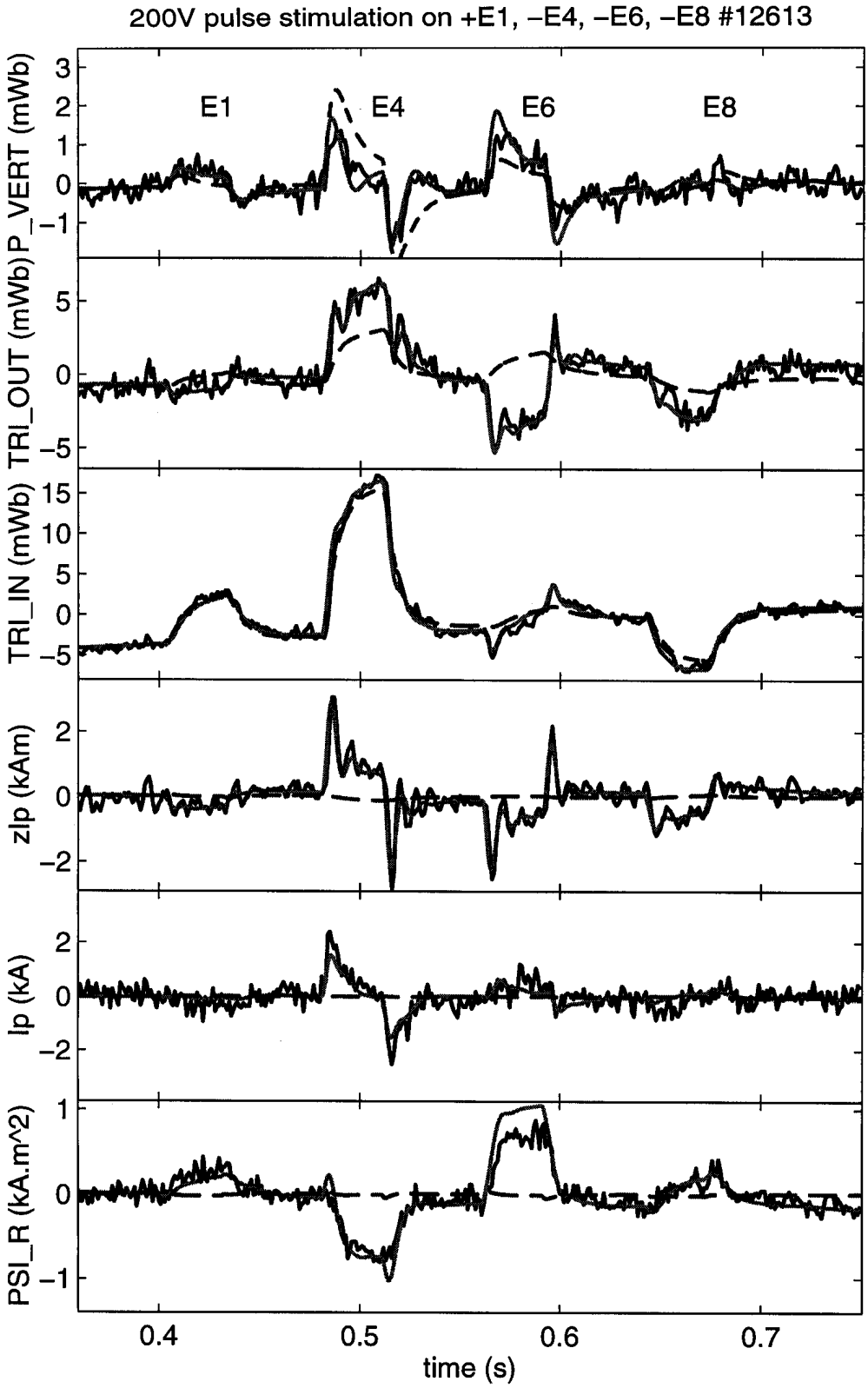

Fig. A8. Comparison of the experimental, CREATE-L and plasmaless CREATE-L responses to square pulse stimulation on the E coils. Experimental response (dark solid), CREATE-L (light), plasmaless CREATE-L (dashed).

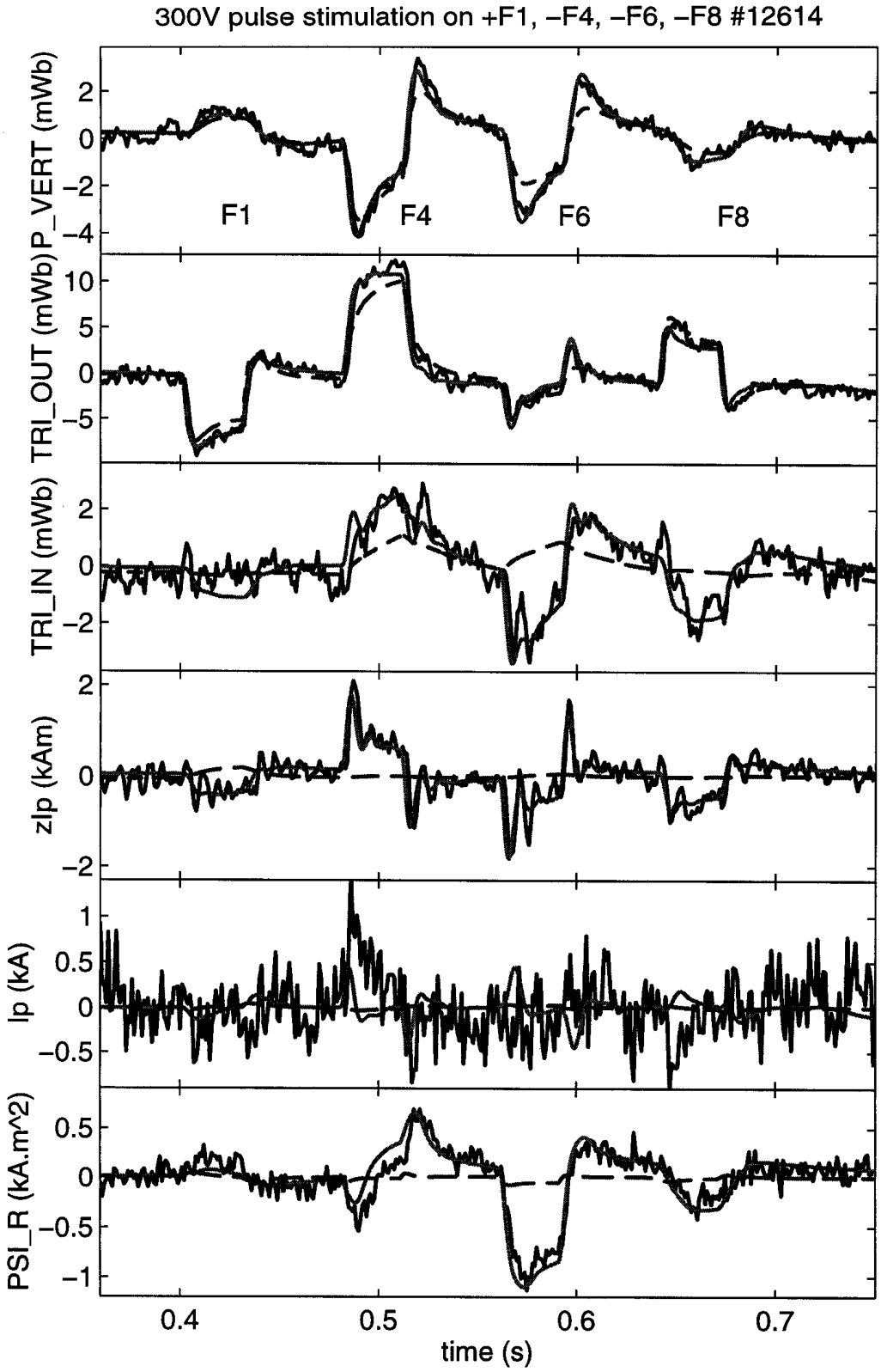

Fig. A9. Comparison of the experimental, CREATE-L and plasmaless CREATE-L responses to square pulse stimulation on the F coils. Experimental response (dark solid), CREATE-L (light), plasmaless CREATE-L (dashed).

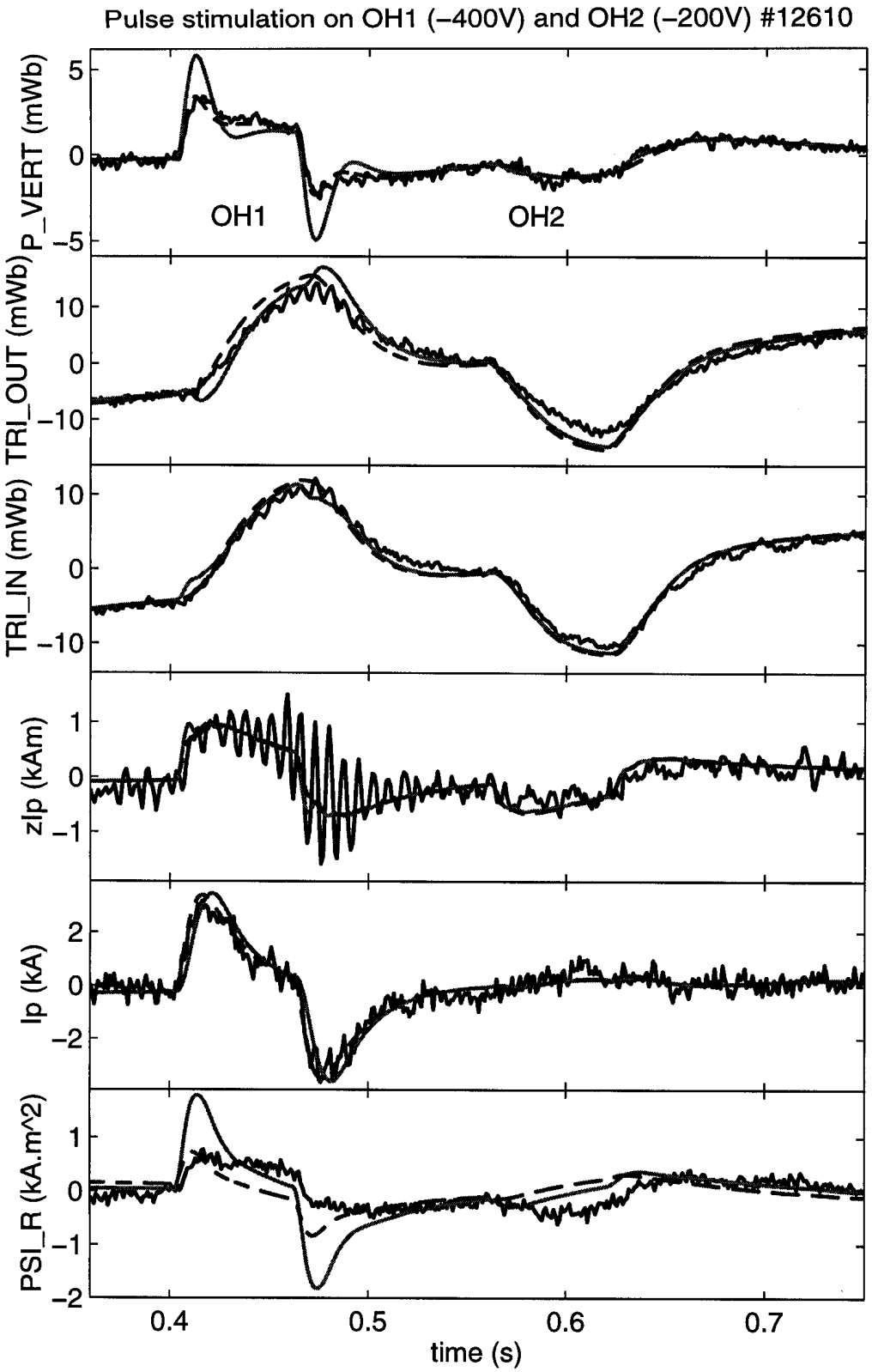

Fig. A10. Comparison of the experimental, frozen flux CREATE-L and limited CREATE-L responses to square pulse stimulation on the OH coils. Experimental response (dark solid), frozen flux CREATE-L (light solid), limited CREATE-L (dashed).

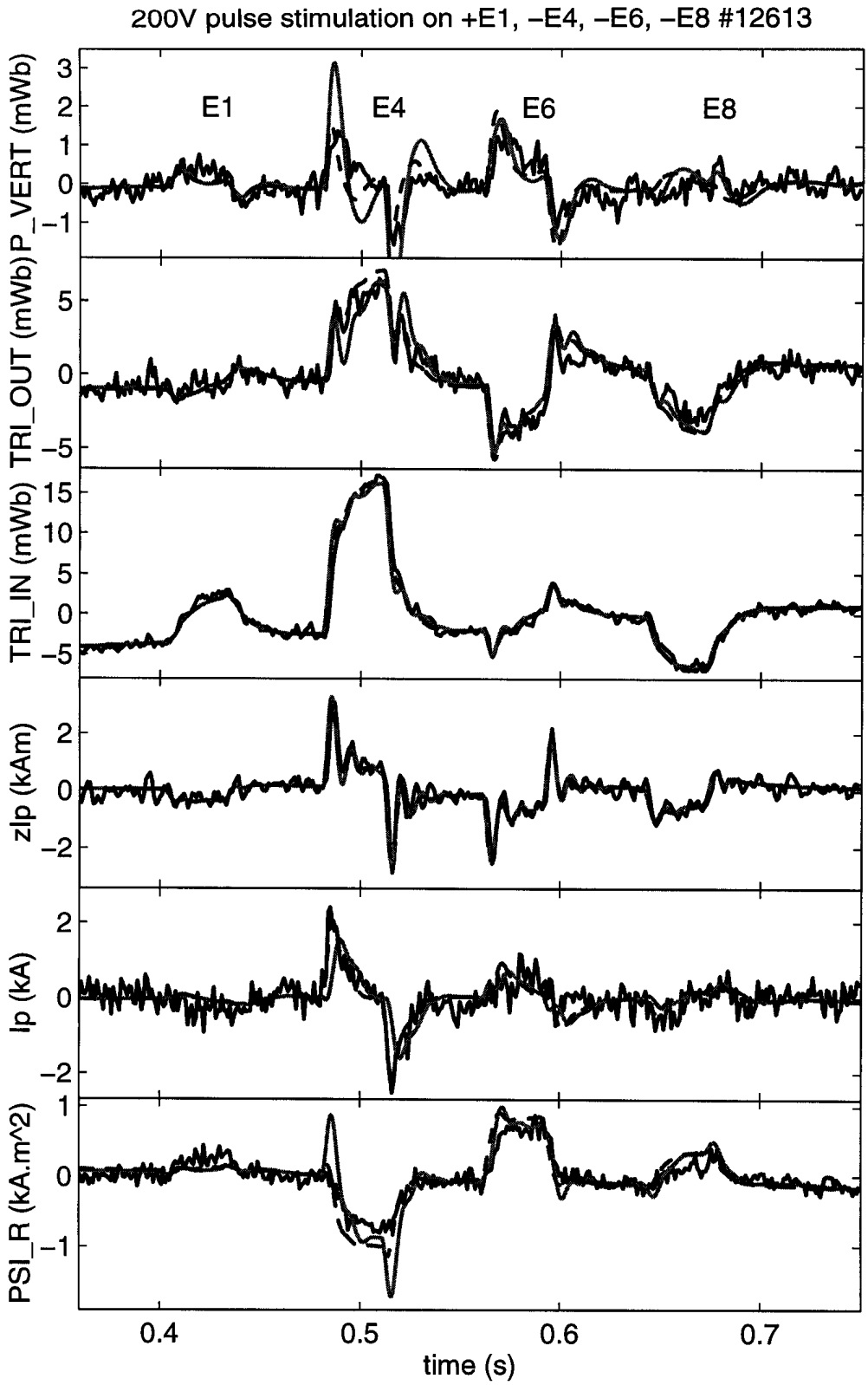

Fig. A11. Comparison of the experimental, frozen flux CREATE-L and limited CREATE-L responses to square pulse stimulation on the E coils. Experimental response (dark solid), frozen flux CREATE-L (light solid), limited CREATE-L (dashed).

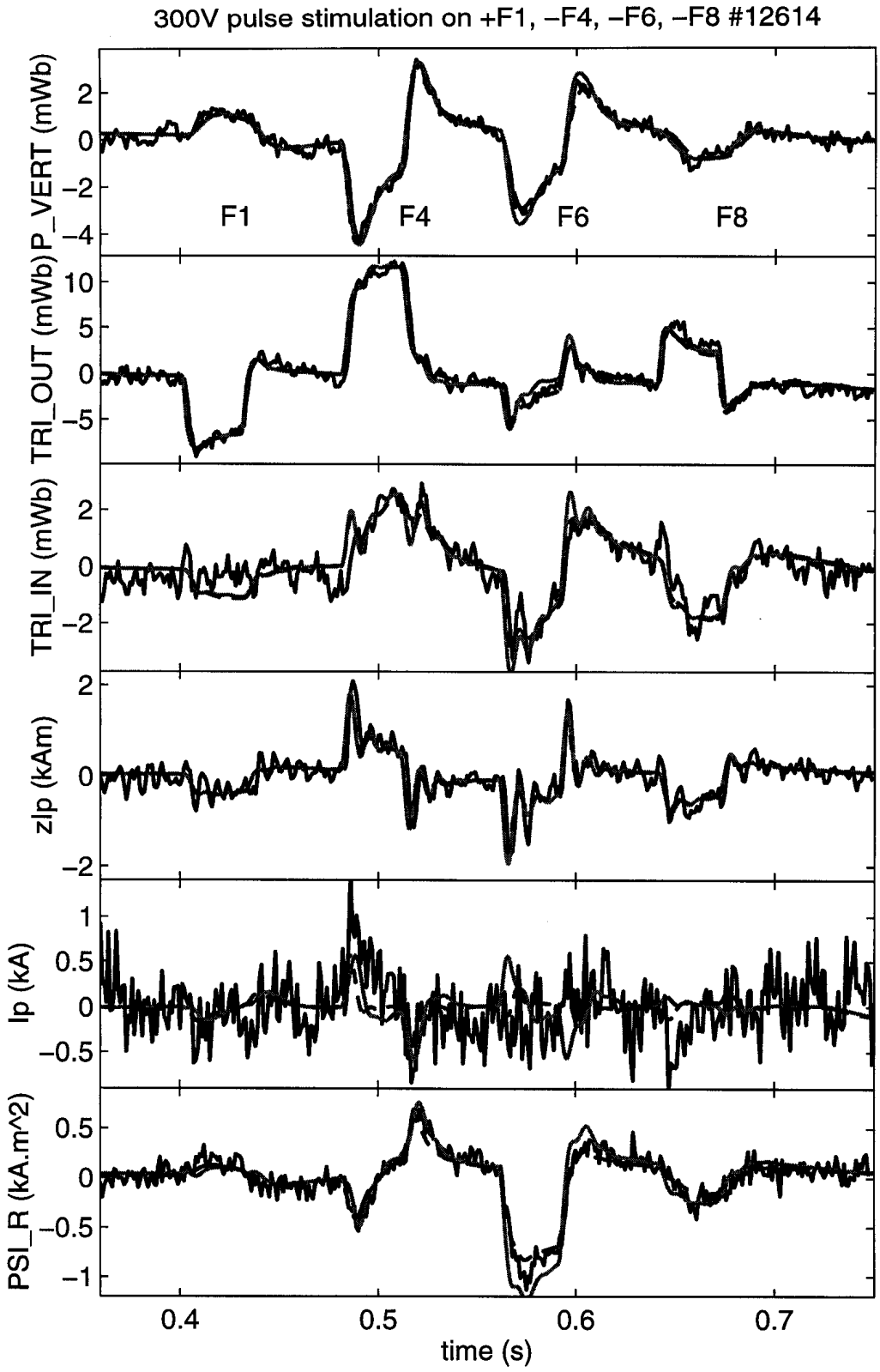

Fig. A12. Comparison of the experimental, frozen flux CREATE-L and limited CREATE-L responses to square pulse stimulation on the F coils. Experimental response (dark solid), frozen flux CREATE-L (light solid), limited CREATE-L (dashed).

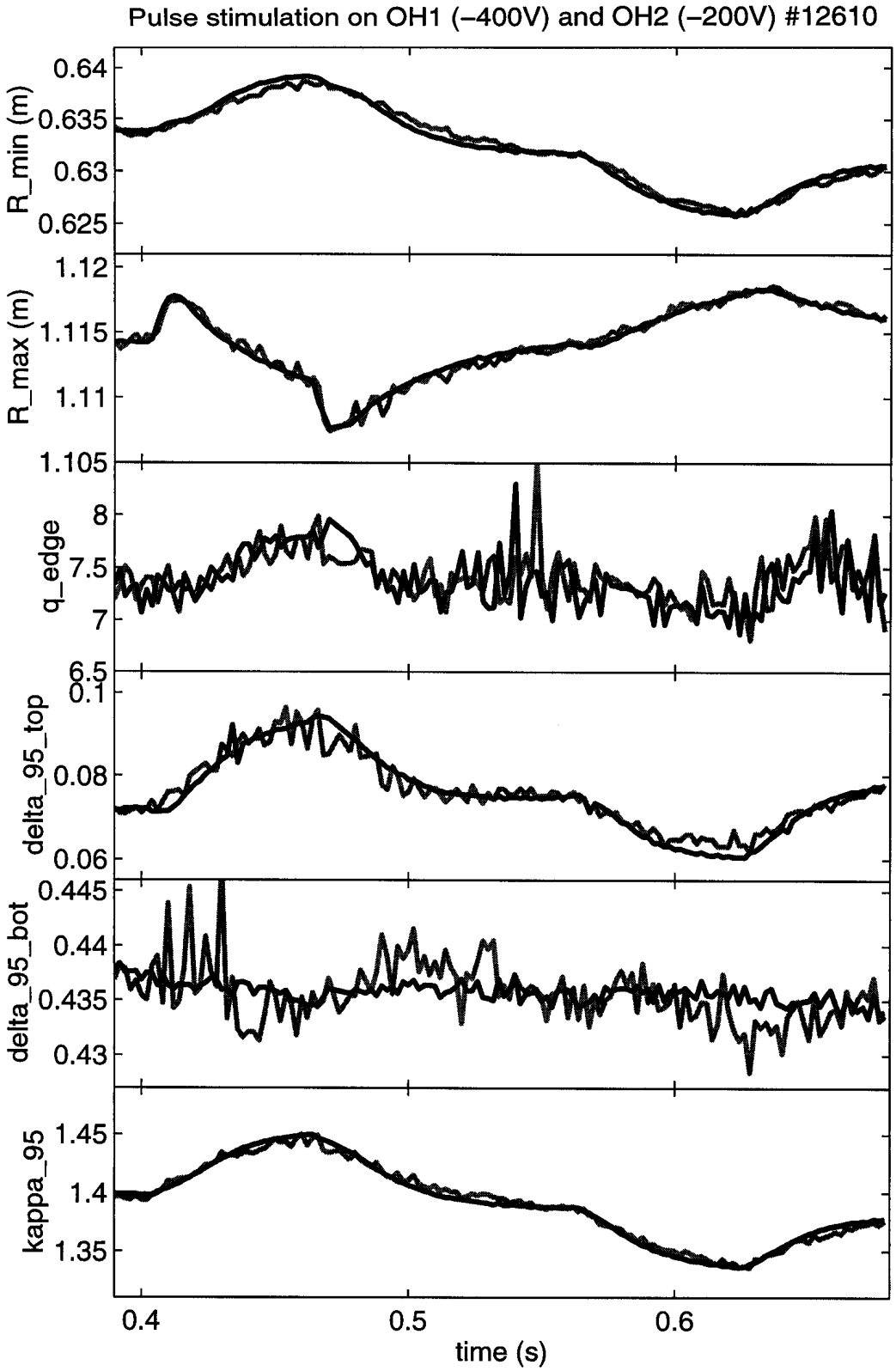

Fig. A13. Reconstructed plasma shape and position parameters showing minimum and maximum radius on plasma last closed flux surface, safety factor (q), elongation (κ) and upper and lower triangularity (δ) at the 95% flux surface. Experimental response (light solid) and CREATE-L (dark solid) to OH coil stimulation.

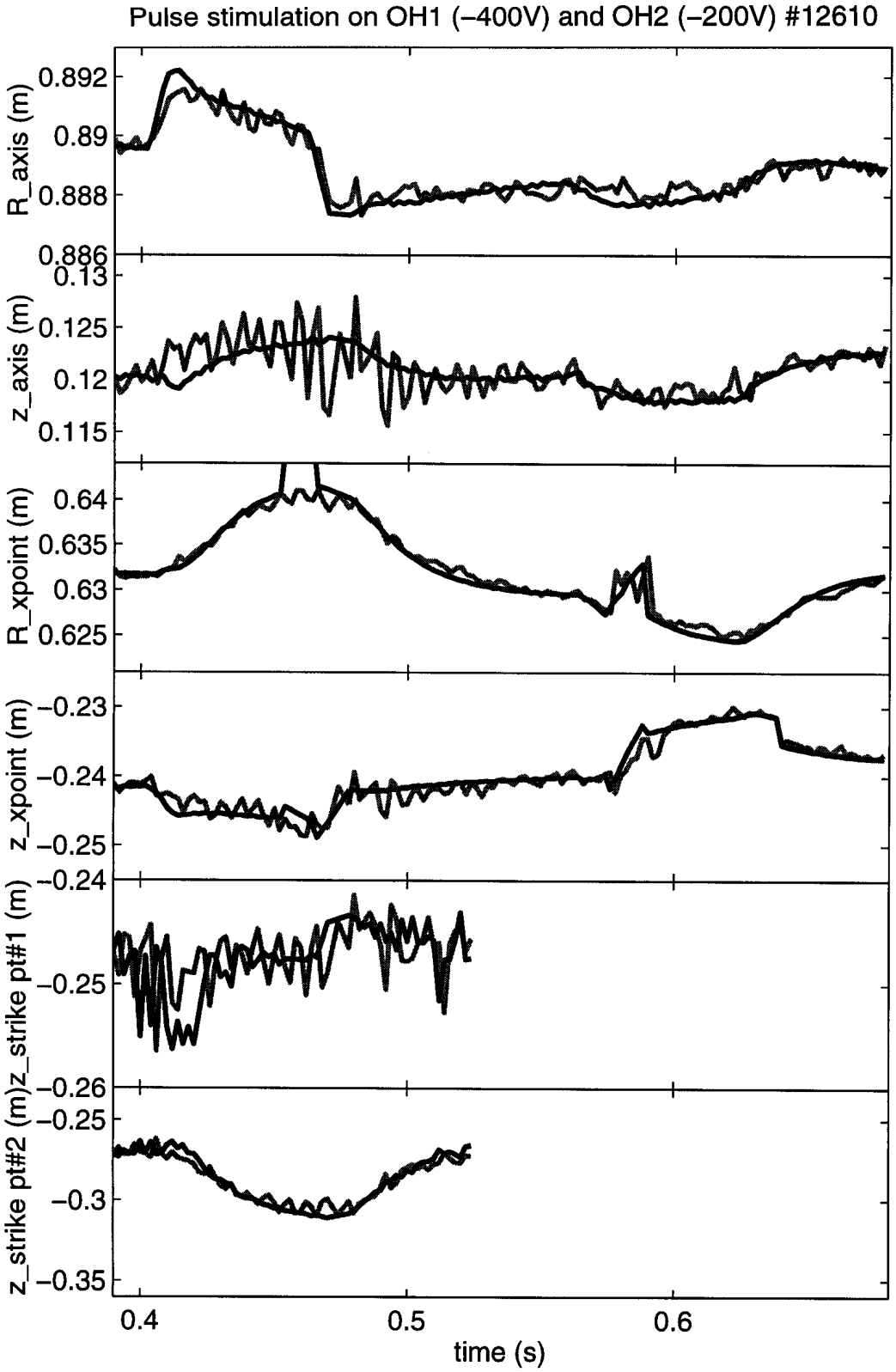

Fig. A14. Reconstructed plasma parameters showing positions of magnetic axis, X-point and strikes points. Experimental response (light solid) and CREATE-L (dark solid) to OH coil stimulation.

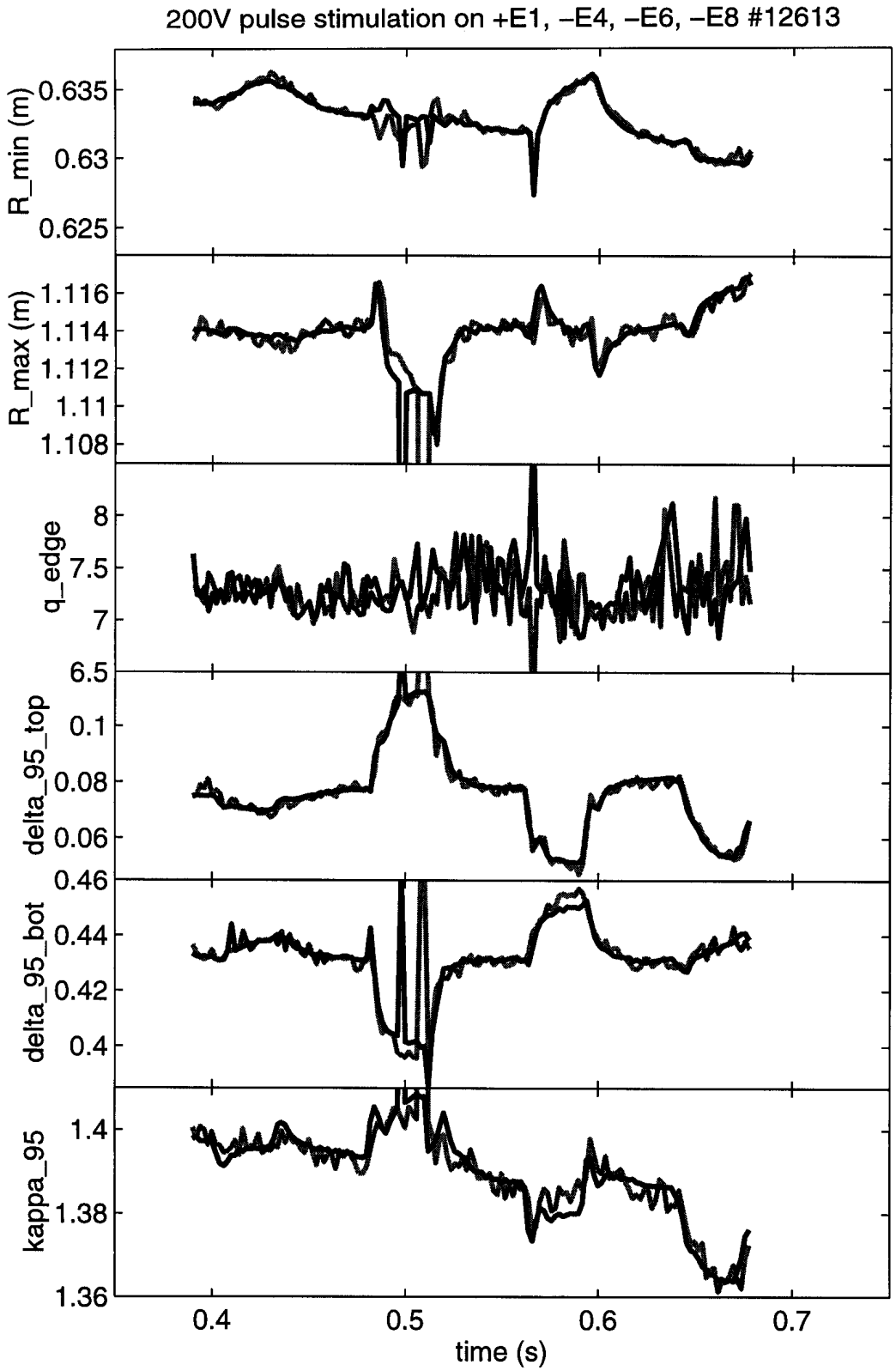

Fig. A15. Reconstructed plasma shape and position parameters showing minimum and maximum radius on plasma last closed flux surface, safety factor (q), elongation (κ) and upper and lower triangularity (δ) at the 95% flux surface. Experimental response (light solid) and CREATE-L (dark solid) to E coil stimulation.

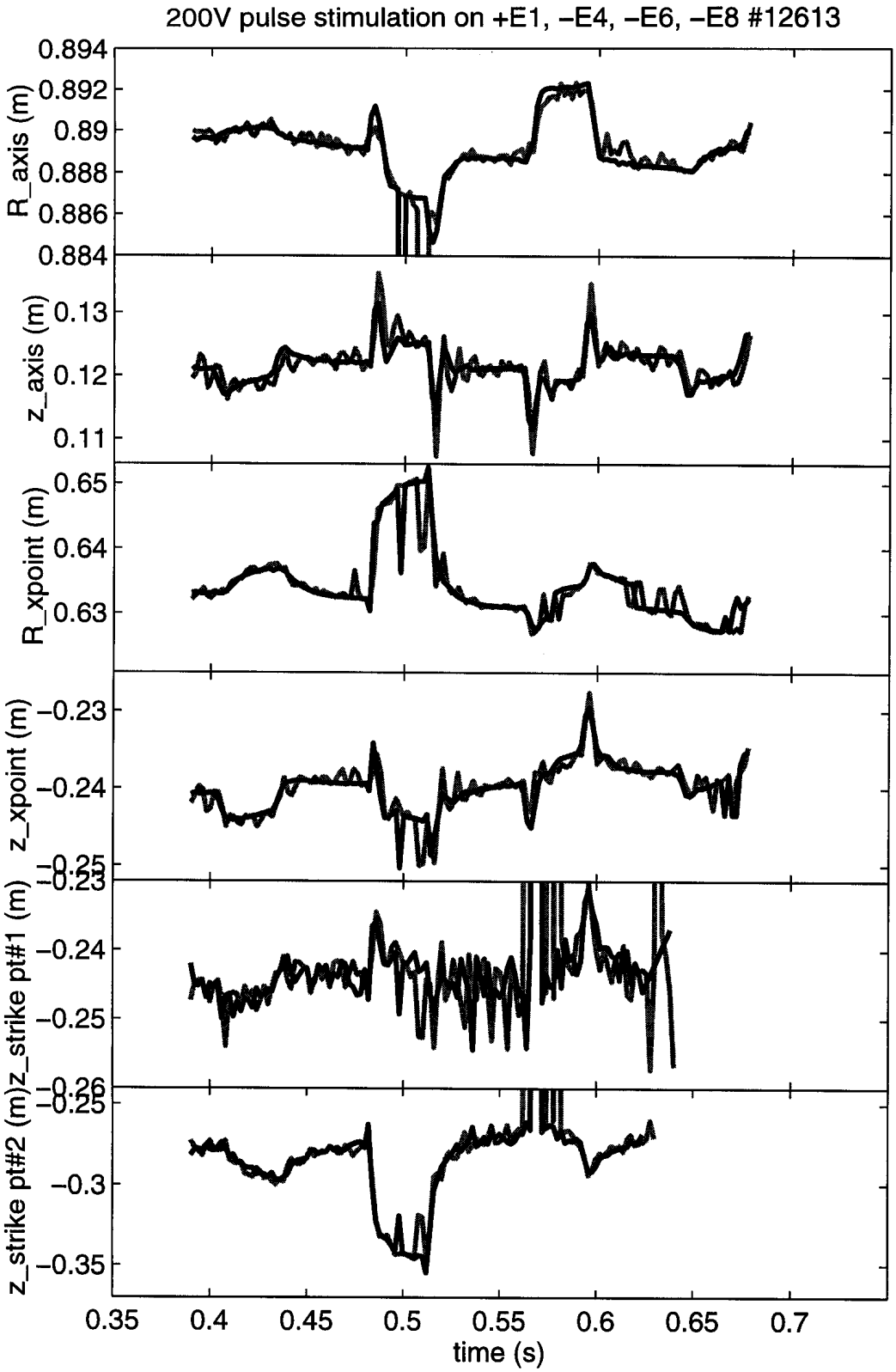

Fig. A16. Reconstructed plasma parameters showing positions of magnetic axis, X-point and strikes points. Experimental response (light solid) and CREATE-L (dark solid) to E coil stimulation.

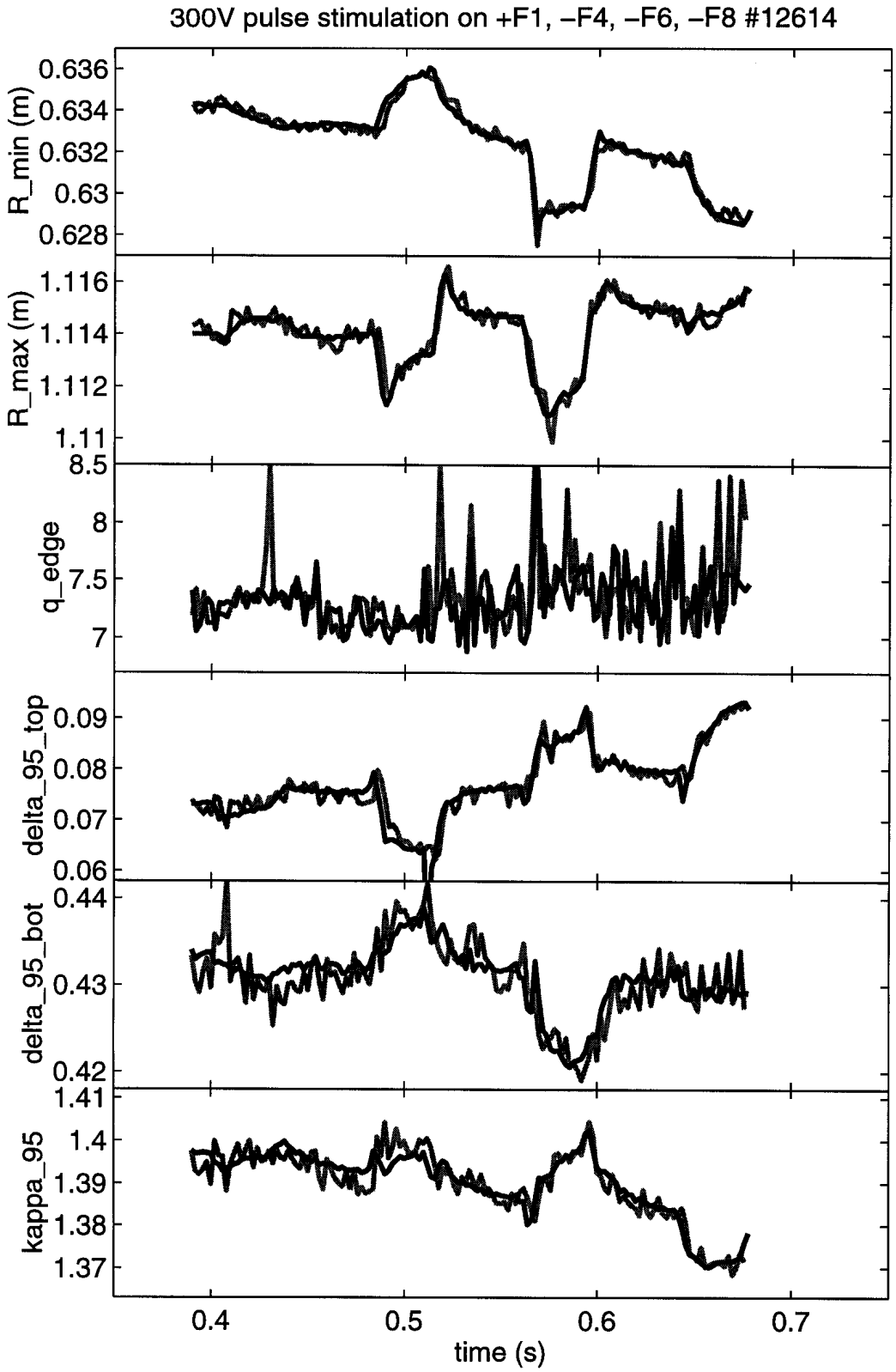

Fig. A17. Reconstructed plasma shape and position parameters showing minimum and maximum radius on plasma last closed flux surface, safety factor (q), elongation (κ) and upper and lower triangularity (δ) at the 95% flux surface. Experimental response (light solid) and CREATE-L (dark solid) to F coil stimulation.

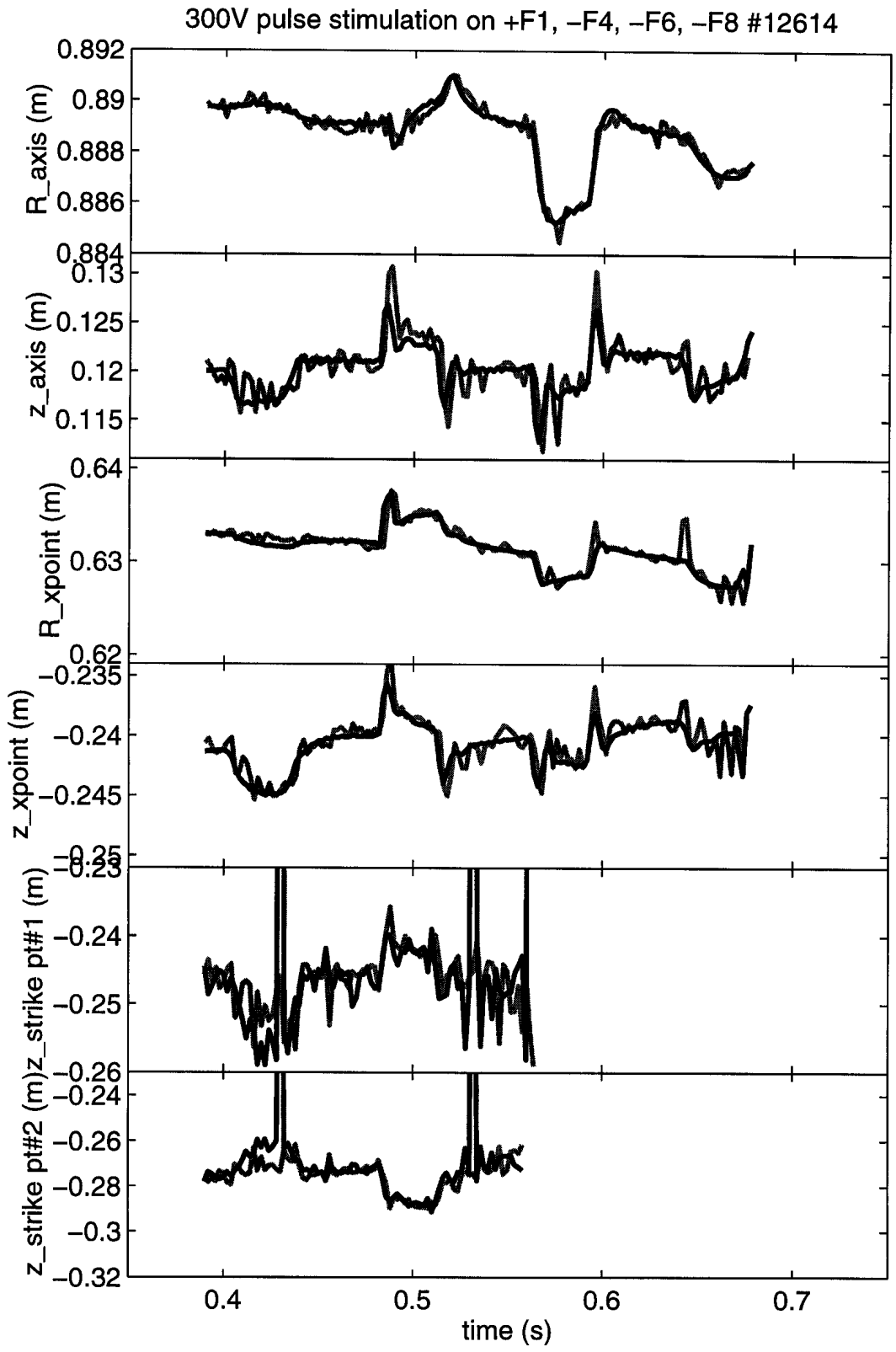

Fig. A18. Reconstructed plasma parameters showing positions of magnetic axis, X-point and strikes points. Experimental response (light solid) and CREATE-L (dark solid) to F coil stimulation.

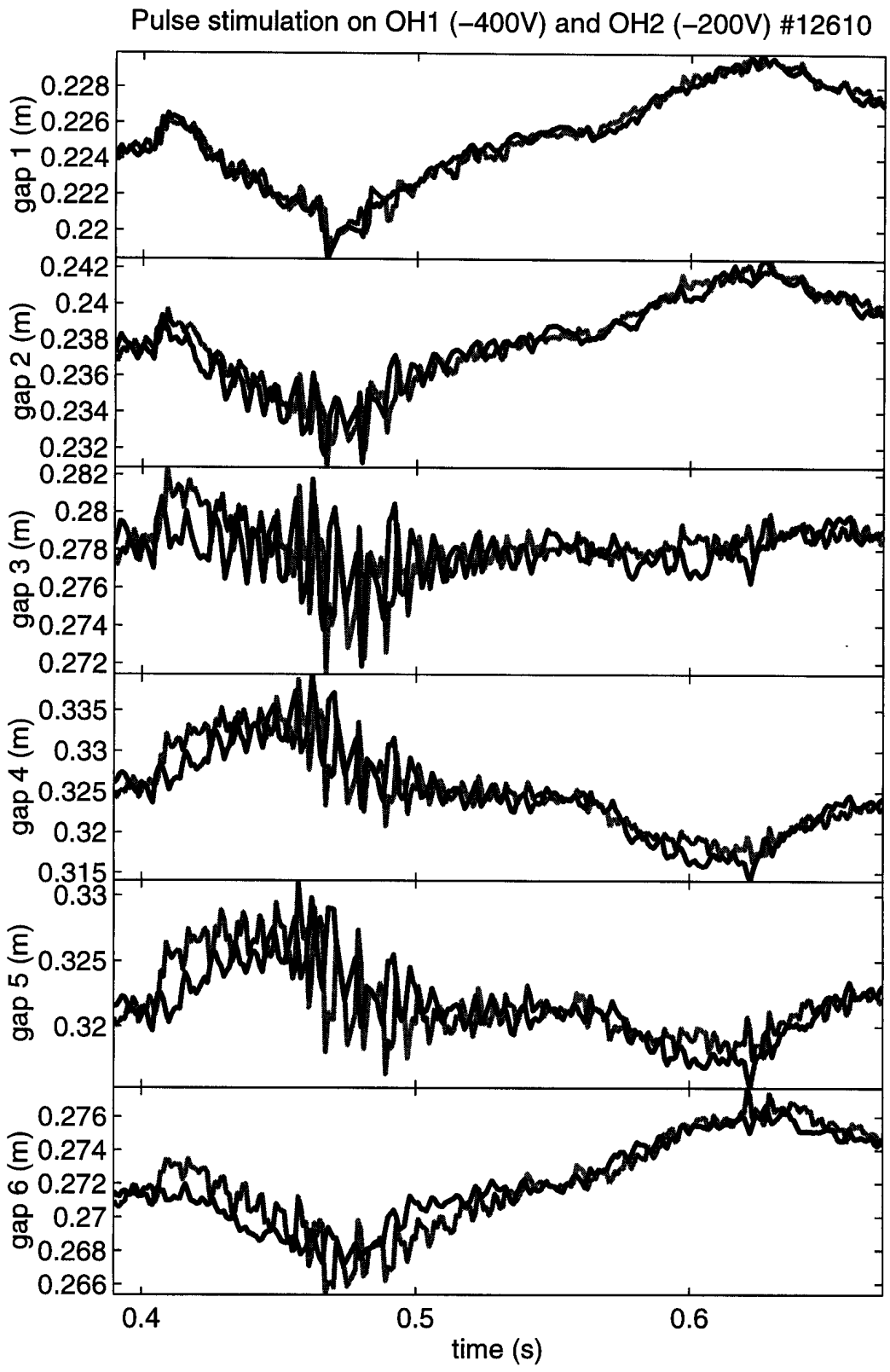

Fig. A19. Reconstructed plasma radii for OH coil stimulation. Experimental response (light solid) and CREATE-L (dark solid).

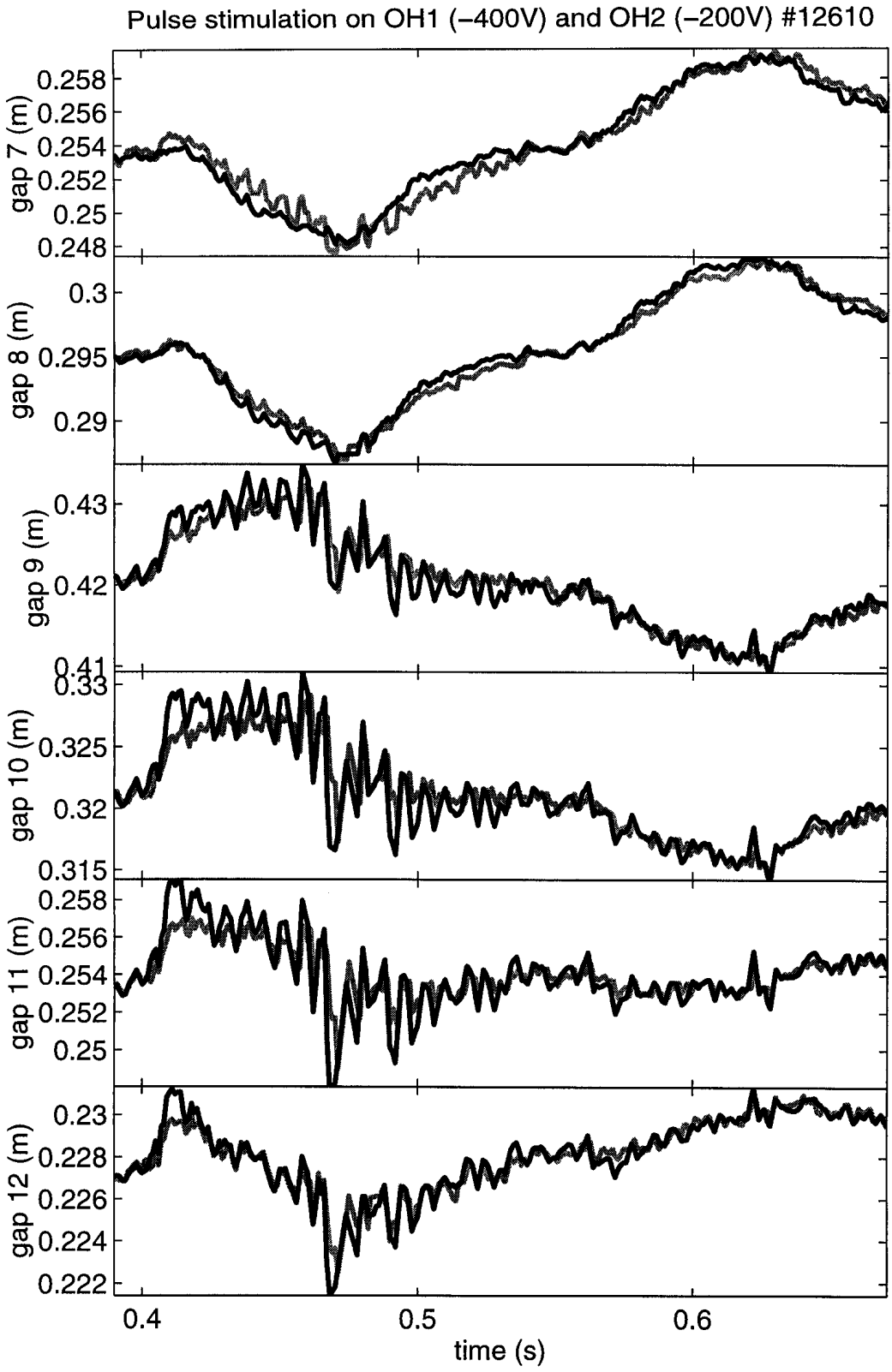

Fig. A20. Reconstructed plasma radii for OH coil stimulation. Experimental response (light solid) and CREATE-L (dark solid).

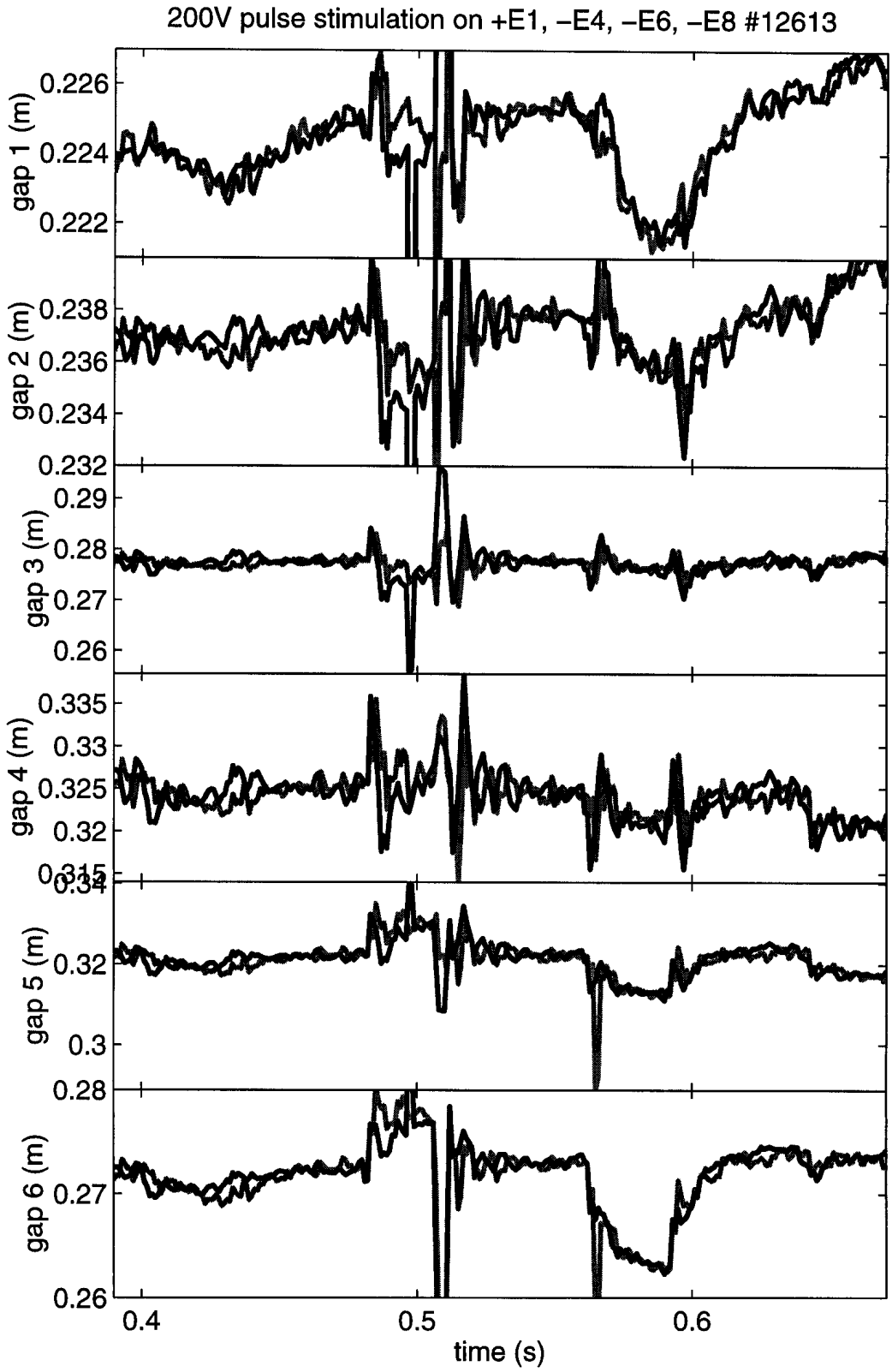

Fig. A21. Reconstructed plasma radii for E coil stimulation. Experimental response (light solid) and CREATE-L (dark solid).

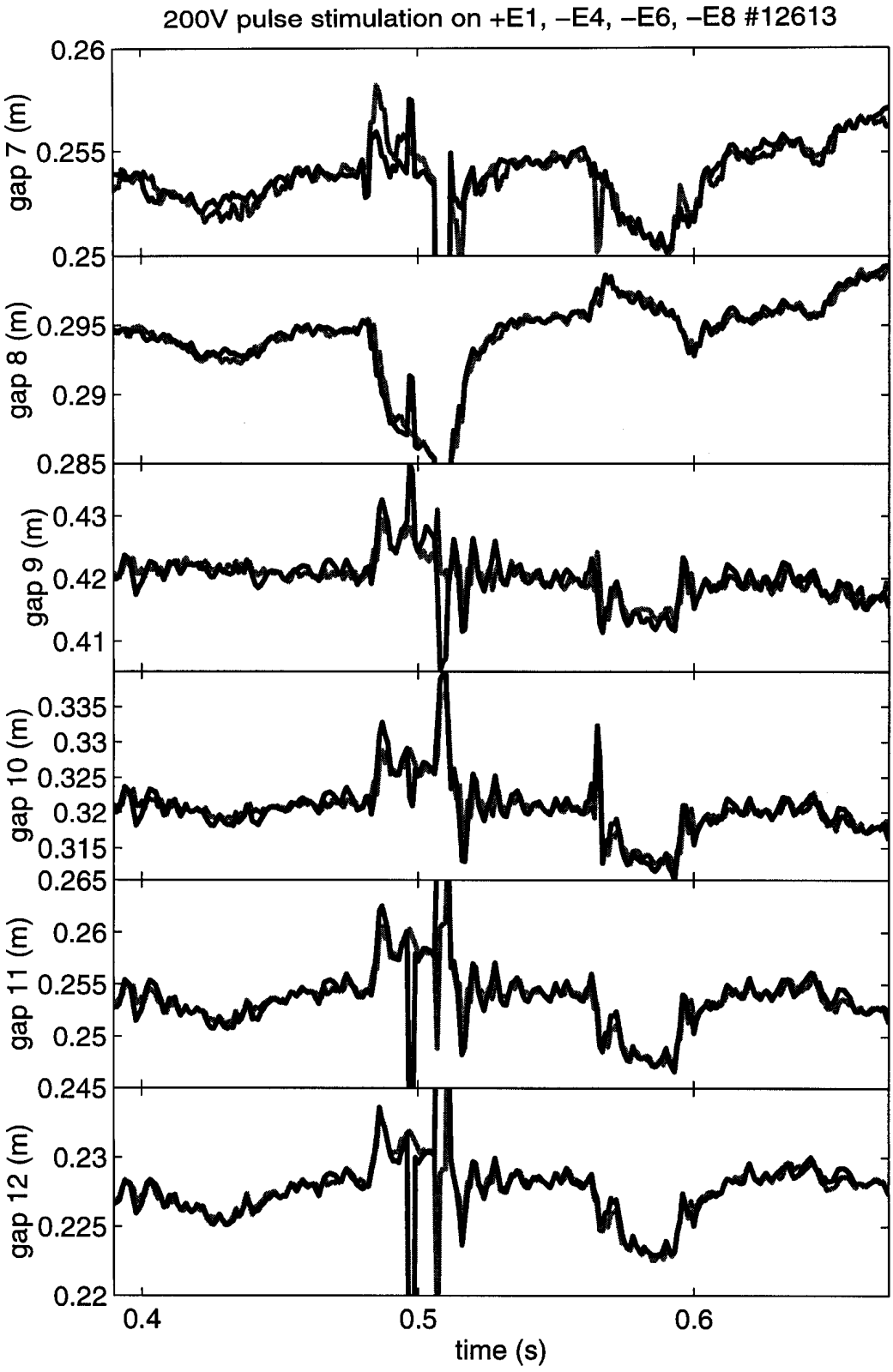

Fig. A22. Reconstructed plasma radii for E coil stimulation. Experimental response (light solid) and CREATE-L (dark solid).

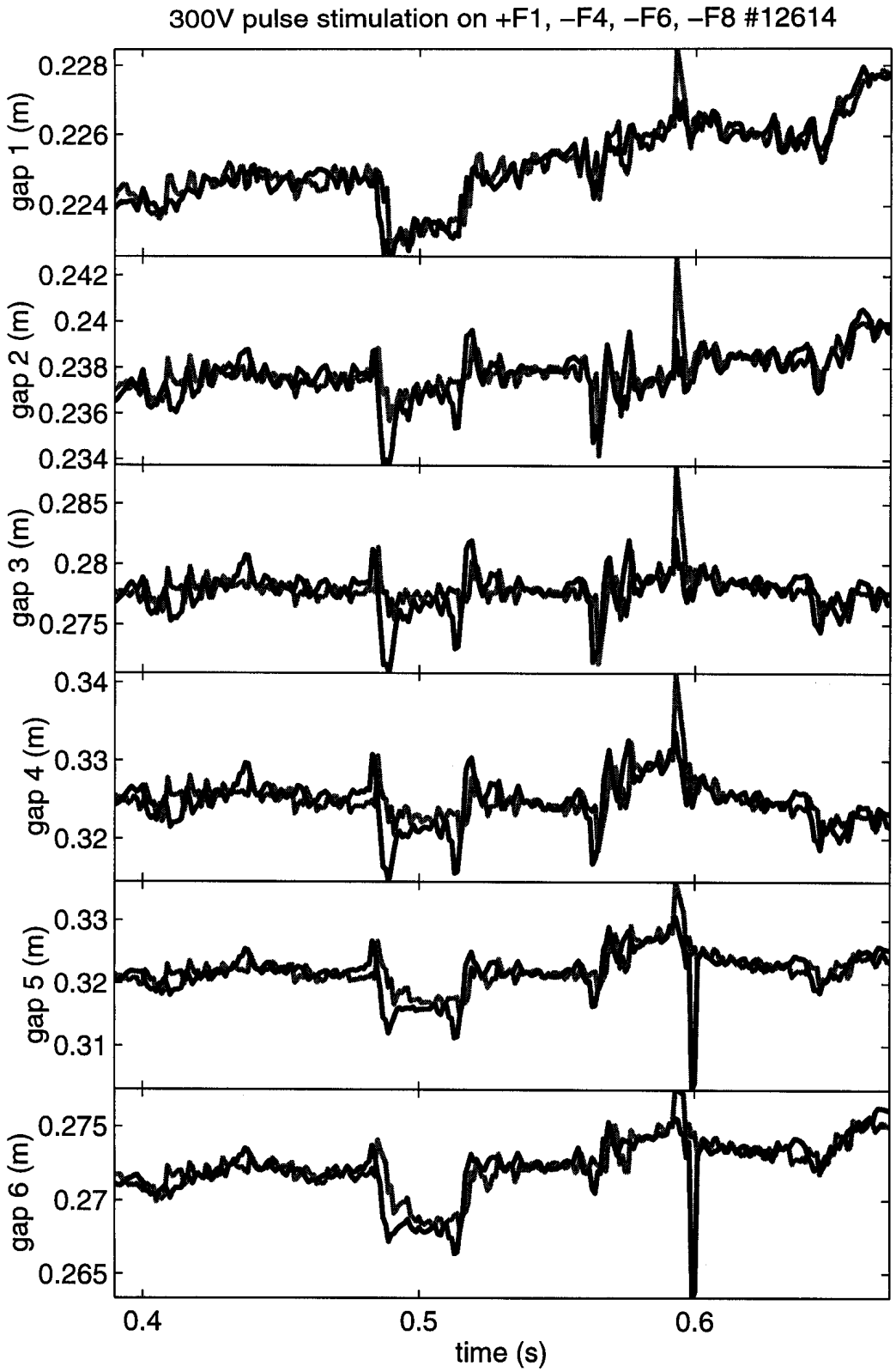

Fig. A23. Reconstructed plasma radii for F coil stimulation. Experimental response (light solid) and CREATE-L (dark solid).

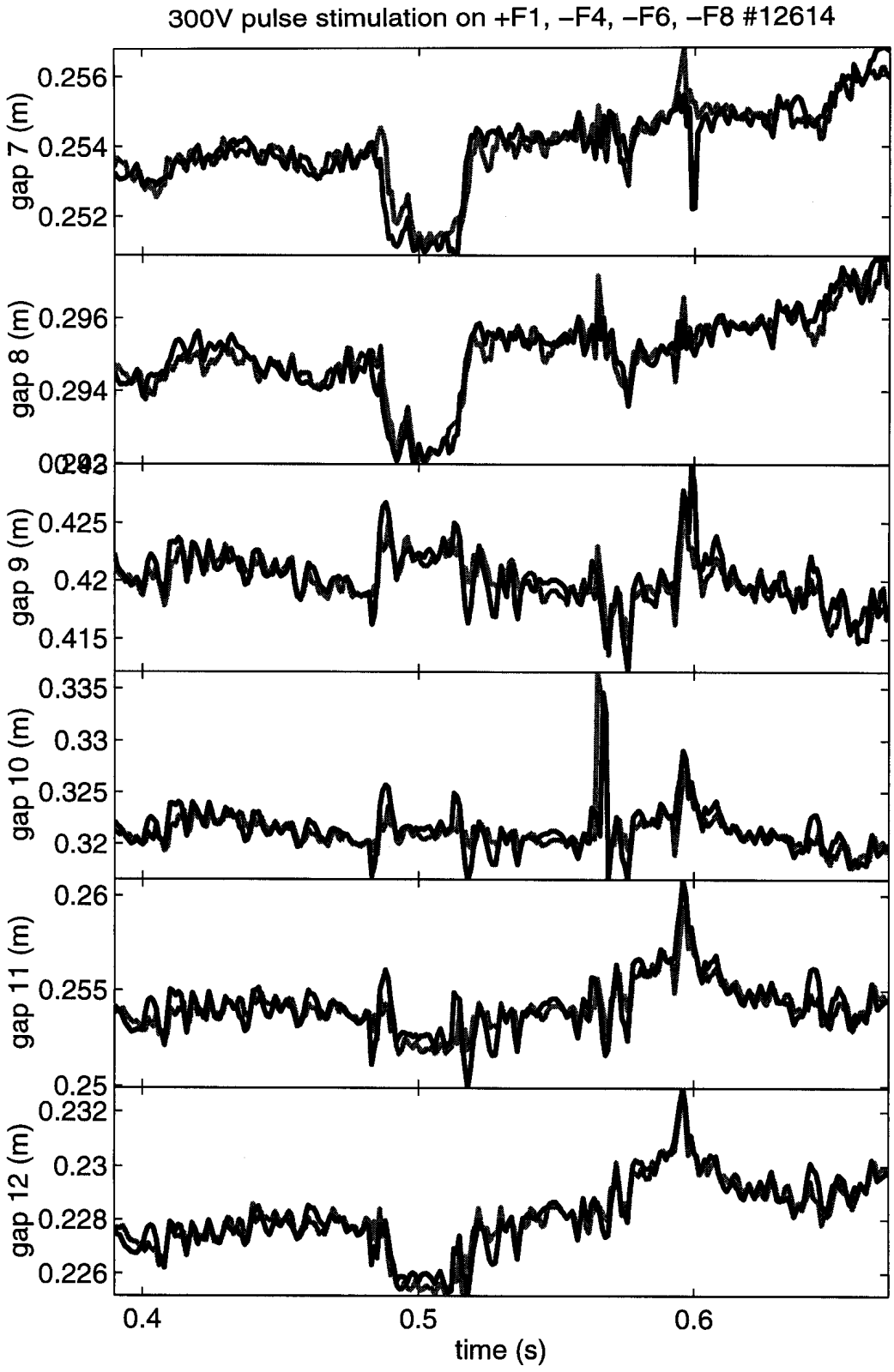

Fig. A24. Reconstructed plasma radii for F coil stimulation. Experimental response (light solid) and CREATE-L (dark solid).